5

RITONAVIR

AND

MSNs

5. Ritonavir and MSNs

Experimental

5.1 Synthesis of Mesoporous Silica Nanoparticles (MSNs)

5.1.1 Materials

Cetyltrimethylammonium bromide (CTAB), tetraethyl ammonium hydroxide (TMAOH), Pluronic P-123, tetraethyl orthosillicate (TEOS), fumed silica, ammonium hydroxide (NH4OH) and ethyl acetate were purchased from Sigma-Aldrich (Ind). Hydrochloride acid (HCl) and methanol (AR grade) were procured from Rankem (India). All other solvents and material were of AR grade and were used as such. Deionized water was utilized in the synthesis of MSNs.

5.1.2 Synthesis procedure for various Mesoporous Silica Nanoparticles (MSNs)

5.1.2.1 Synthesis of MCM-41NPs

The MCM-41NPs synthesized was carried out as per the procedure given in the literature[1]. Accurately weighted 4.42 g of CTAB was added in 36 g of deionized water and stirred for 15 min. Then add slowly 3.46 g TMAOH in the surfactant solution of CTAB with consistent stirring. The obtained mixture was stirred for 30 min. Then gently added 3 g of fumed silica with continued stirred for 1.5 h. The obtained gel was treated by hydrothermal crystallization technique for 48 h at 110°C in a reactor. Afterword, by filtration process the solid product was recovered and washed it with deionized water and kept at room temp overnight. Further removal of surfactant was carried out by calcination of the product in a muffle furnace at 550 °C for 6 h. The recovered final product was named as MCM-41NPs.

5.1.2.2 Synthesis of MCM-48NPs

The MCM-48NPs synthesis was carried out as per the procedure given in the literature[2]. Weighted 0.4 g CTAB was added in 30 mL of methanol-water (1:2) solution and stirred the solution for 15 min. Then 1.7 mL ethyl acetate and 5.4 mL ammonium hydroxide (NH4OH) were added in above solution and stirred it for 10 min. afterward, 0.9 mL TEOS was slowly added into the solution with continuous stirring. Further; 150 mL water was added into the solution and kept it overnight with continue stirring at room temperature. Then the resulting solid sample was recovered by filtration and washed it with methanol. Then recovered solid product dried in an oven at 60ºC for overnight. Then the final product was calcined in a muffle furnace for removing of surfactant at 550°C for 6 h. Recovered material was labeled as MCM-48NPs.

5.1.2.3 Synthesis of SBA-15NPs

The SBA-15NPs synthesis was carried out as per the procedure reported in the literature[3]. Accurately weighted 8g of P-123 was added in 260 g of deionized water, stirred it for 15 min. Then 40 ml HCl (37%) was added into the surfactant solution of P-123 and continuous stirred for 1h. Then slowly added 18.28 ml of TEOS and stirred continued for 8h at 45°C. The obtained mixture was kept at 100°C for 72h in a reactor for hydrothermal crystallization treatment. After that; by simple filtration process the solid product was recovered and washed it with deionized water and kept in the oven at 80°C temp for overnight. Further removal of surfactant was carried out by calcination of the product in a muffle furnace at 550°C for 6 h. The recovered final product was labeled as SBA-15NPs.

5.2 Characterization of synthesized MSNs

The synthesized MSNs were identified and characterized by different instrumental and analytical techniques, to understand different physicochemical features of these nanoparticles.

5.2.1 Scanning Electron Microscopy (SEM)

The morphological study of different synthesized MSNs was determined by SEM operated at an acceleration voltage of 15 kV. The MSNs samples were affixed to an aluminum stub by using carbon tape and gold coating was done with ion sputter MC1000. The samples were analyzed by using a Hitachi-SU 1510 microscope.

5.2.2 Transmission Electron Microscopy (TEM)

The porous framework and particle size of MSNs were confirmed by TEM Analysis. TEM images of MSNs were taken with a TECHNAI-G2 Spirit-Biotwin, operated at 120 kV. The MSNs samples were dispersed in deionized water and sonicated for ten minutes. Several drops of these samples were deposited on 200 mesh, copper grid coated with a holey carbon film. The images were recorded on electron negative films.

5.2.3 FT-IR analysis

FT-IR spectra of MSNs were recorded on a BRUKER ALPHA-T (GERMANY) FT-IR Spectrophotometer. The samples were gently mixed with KBr powder in mortar. Then pallets were prepared under 5000 psi pressure. The IR spectra of samples were taken in the spectral region 4,000 to 700 cm−1 using the resolution 1 cm−1.

5.2.4 Differential Scanning Calorimetry (DSC)

To study the physical state of MCM-41NPs, MCM-48NPs, and SBA-15NPs were examined by DSC on a Shimadzu DSC-60. Around 3-5 mg of samples were put into an aluminum pan, crimped it with an aluminum lid to provide an adequate seal and

heated under nitrogen purging (flow rate 40 mL/min) from room temperature to 300°C. The temperature rise rate was fixed at 10°C/min. DSC thermogram were analyzed using TA 60-WS software.

5.2.5 Powder X-ray diffraction (PXRD)

The crystalline arrangements and the nature of MCM-41NPs, MCM-48NPs and SBA-15NPs (MSNs) were studied using a powder X-ray diffractometer (EMPYREAN, PANalytical) using Cu Kὰ radiation beam operating at 40kV and 30mA. The MSNs samples were scanned at a low angle from 1 to 10 degrees in continuous mode at scanning speed 0.02 2θ/5s and also RTV and R-MSNs scanned from 5 to 50 degrees in continuous mode.

5.2.6 N2 Adsorption-desorption analysis

N2 adsorption and desorption analysis is a most reliable method to study the porosity of mesoporous material and was carried out to get information regarding BET surface area, pore size (nm) and pore volume of different synthesized MSNs by using Micromeritics ASAP 2010. Earlier to characterization, all plain MSNs samples were degassed under vacuum at 200°C for 5h, The BET specific surface area was calculated by application of the BET method to the isotherm. The pore volume and pore diameter of all plain MSNs were calculated by application of Barrett–Joyner–Halenda (BJH) method to the isotherm.

Optimization of drug loading procedure

The drug loading process was optimized with respect to drug: carrier ratio.

Ratio of drug as to carrier

Another important parameter is to select the proper ratio of drug (RTV) and drug carriers (MCM-41NPs, MCM-48NPs and SBA-15NPs) for maximum entrapment. Different ratios were tried and checked for drug loading. Also the effect of different solvents, stirring rate and time effect on drug loading was also checked.

5.3 RTV loading in mesoporous silica nanoparticles (MSNs)

MCM-41NPs, MCM-48Nps and SBA-15NPs (MSNs) were used for drug loading process. All MSNs were dried at 80°C for 30 min, to remove the moisture contain from the pores of mesostructure before loading the drug into the mesopores. Different drug loading methods were used for RTV e.g. like Adsorption equilibrium method, Fusion method and solvent evaporation method. Ultimately, solvent evaporation technique was used for drug loading. In preliminary RTV loading procedure, RTV (100mg) was dissolved in methanol (10 ml) and then MCM-41NPs

(150 mg) was added slowly. The mixture was stirred for 1-2h at room temperature for achieving maximum drug loading and then the methanol was recovered by solvent evaporation method at 50°C on Bucchi rotary evaporator until complete dry powder of MCM-41NPs was obtained. The recovered solid drug loaded R-MCM-41NPs was dried at room temperature and stored in a dry place for further use.

The similar procedure was used for the RTV loading in MCM-48NPs and SBA-15NPs. And the products were named as R-MCM-48NPs and R-SBA-15NPs. All RTV loaded mesoporous silica nanoparticles designated as R-MSNs-NPs

5.4 Characterization of RTV loaded Mesoporous silica nanoparticles (R-MSNs-NPs)

The RTV loaded MSNs (MCM-41NPs, MCM-48NPs and SBA-15NPs) were analyzed by TEM, DSC, FT-IR, powder-XRD and N2-adsorption isotherm that specify the specific surface area, pore diameter and pore volume. The entrapment efficiency (EE) and loading efficiency (LE) for different MSNs were determined indirectly using UV spectrophotometric method at 240nm wavelength.

10mg of RTV loaded different MSNs were dispersed in a 10ml volume of methanol respectively and mixed thoroughly so that the RTV gets solubilized into the methanol and then subsequent filtration of the sample was carried out. The amount of drug loaded was calculated using the standard calibration curve.

The loading efficiency was again confirmed by Thermogravimetric analysis on Shimadzu TGA-50. Around 3-10 mg sample of RTV and R-MSNs were kept into the platinum pan respectively, then heated up to 500 °C at a scanning rate of 10 °C/min under a nitrogen gas flow of 50 mL/min. The thermograms were analyzed using the TA-60 software.

The % entrapment efficiency for RTV and % loading efficiency for MSNs were calculated by using a formula:

$$\% \text{ Entrapment efficiency (\% EE)} = \frac{\text{Weight of RTV in nanoparticles}}{\text{Weight of RTV initially added}} * 100 \quad \text{---- (1)}$$

$$\% \text{ Loading Efficiency (\% LE)} = \frac{\text{Weight of RTV in nanoparticles}}{\text{Total weight of sample}} * 100 \quad \text{----- (2)}$$

5.5 Formulation of R-MSNs tablet and evaluation

For *In vitro* dissolution study drug loaded mesoporous silica nanoparticles were formulated in tablets by direct compression method. R-MCM-41NPs equivalent to 100 mg RTV and different excipients like Low- Hydroxypropyl cellulose (L-HPC),

microcrystalline cellulose, cross-povidone, lactose monohydrate (SUPERTAB 11SD) and magnesium stearate were blended and punched in single punch tablet machine having 12 mm diameter punches with flat faced beveled edges.[4,5] The same procedure was followed for R-MCM-48NPs and R-SBA-15NPs for preparations of tablets. All prepared tablets were evaluated for various parameters such as weight variation, hardness, friability and disintegration time etc. The excipients used to formulate tablets were of 'GRAS' (Generally Regarded as Safe) category and are also used to prepare RTV MF.[4, 5] Ritonavir tablet formulation composition are given below in table 5.1

Table 5.1Ritonavir Tablet Formulation Composition

Ingredients	Quantity (mg/tablet)
R-MCM-41NPs*	250
microcrystalline cellulose PH102	120
lactose monohydrate (SUPERTAB 11SD)	75
cross-povidone	25
Low-Hydroxypropyl cellulose (L-HPC)	25
magnesium stearate	5
Total weight	**500**

*Remarks: For MCM-48 and SBA-15 nanoparticles equivalent to 100 mg Ritonavir were taken and tablet weight was adjusted with Microcrystalline cellulose PH 102.

5.6 *In-vitro* dissolution study

In-vitro dissolution study was performed in dissolution apparatus (Veego dissolution test apparatus). Six dissolution units were studied for In-vitro dissolution of the RTV pure drug and R-MSNs. R-MCM-41NPs, R-MCM-48NPs and R-SBA-15NPs equivalent to 100 mg tablets of RTV, pure drug RTV tablets and marketed formulation (MF) were taken for the in-vitro dissolution study. *In vitro* dissolution studies were conducted in the (a) pH 1.2±0.1 hydrochloric acid solution (0.1N HCl), (b) Acetate buffer pH 4.5 with 0.75% PLE and (c) Phosphate buffer pH 6.8 with 0.75% PLE media using USP dissolution apparatus II, with paddle rotating speed 50rpm in 900 mL media volume at 37±0.5°C temperature. At predetermined time intervals of 10, 20, 30, 45 and 60 min, five mL of dissolution sample was removed from the vessels with the help of cannula, replacing the same amount with fresh dissolution medium. Samples were filtered through 0.22 µm syringe filter and RTV content was determined by RP-HPLC method.

5.7 In-vivo pharmacokinetic study for RTV

Pharmacokinetics (PK) has emerged as an integral part of drug and formulation development, especially when identifying a drug's biological properties. The most

important property of any non-intravenous dosage form, especially oral formulations, intended to treat a systemic condition, is the ability to deliver the active ingredient to the bloodstream in an amount sufficient to cause the desired response. The property of a dosage form has historically been identified as physiologic availability, biologic availability or bioavailability. Bioavailability quantifies the proportion of a drug which is absorbed and available to produce systemic effect. Drug taking orally is most preferable route of administration because number of benefits like ease of compliance, convenience, availability to large population, and cost effectiveness. Oral administration is regarded as the preferred route of drug administration, offering numerous benefits including, convenience, ease of compliance, availability to large population, and cost effectiveness. Oral bioavailability depends on number of factors like aqueous solubility, dissolution rate, presystemic metabolism, first pass metabolism and susceptibility to efflux mechanisms. Thus, only in vitro evaluation will not be able to predict exact role of nanosizing approach in improving bioavailability. Hence, to find exact improvement in bioavailability, pharmacokinetic studies must be performed. In these studies, pharmacokinetic behaviors of the prepared R-MSNs, plain drug and MF were investigated to know the effect and advantages of nanosizing on oral bioavailability of RTV. Non compartmental pharmacokinetic analysis was performed. In the PK study, parameters like Cmax, tmax, t1/2 and Area Under Curve (AUC) were calculated by using plasma concentration Vs time profile curve and results are shown as mean±SD.

5.7.1 Animals

The PK study was performed in Albino wistar rats (weighted-250–300 g, either sex). The animals were maintained on a standard diet with free access to water and housed into groups of two. Animals were kept at normal environment conditions (i.e. 22°C±2°C temperature and 55%±10% RH) under 12 h light/dark conditions. Animal handling routines were performed according to Good Laboratory Practice. The research protocol of the animal study was approved by the Committee for the Purpose of Control and Supervision of Experiments on Animals (CPCSEA), Ministry of Environment and Forest, Govt. of India, India and Institutional Animal Ethics Committee (IAEC) (MSU/IAEC/2014-15/1404), Pharmacy Department, The M.S. University of Baroda, Vadodara, India.

5.7.2 Experimental: Dosing and sampling

Relative bioavailability of R-MSNs was evaluated by comparing the bioavailability of R-MSNs with bioavailability of plain RTV and MF. Animals were divided in five treatment groups and each group contained 3 rats. The animals were fasted over night prior to the experiment with free access of water. The R-MCM-48NPs, R-MCM-41NPs and R-SBA-15NPs (R-MSNs), plain RTV and MF (equivalent to 10 mg/kg of RTV) were dispersed in 2 mL of CMC solution (0.5 % w/v) and administrated orally. Blood was withdrawn from retro-orbital plexus using light ether anaesthesia. Blood samples (0.3 mL) were collected into 60 µL EDTA (0.5 %w/v) containing micro centrifuge tubes at 0, 0.5, 1, 1.5, 2, 4, 6, 8 and 12 h after administration. Collected blood samples were mixed with the anticoagulant by properly shaking and centrifuged at 5000 rpm for 10 min at 4 ºC using a high-speed centrifuge machine and then plasma samples were collected and stored at -20 °C.

5.7.3 Instrumental and statistical analysis

Collected plasma samples were extracted and analyzed by using developed RP-HPLC method (Chapter 3, Section 3.1.3.1). The drug plasma concentrations were determined from the calibration curve. Non-compartmental trapezoidal method was used to calculate the area under the curve (AUC) of plasma concentration as a function of time (t). All data were reported as mean ± SD.

5.8 Cell Line Studies of RTV and it's formulations using Caco-2 cell line model

Human *in vivo* studies are often presumed to serve as the gold standard to assess product bioequivalence (BE), permeability and toxicity of solid oral dosage forms. However, when this general assumption is revisited, it appears that *in vitro* studies are sometimes better than *in vivo* in assessing the BE, permeability and toxicity of solid oral dosage forms. Reason for *in vitro* studies to serve as better method are that *in vitro* studies: (a) reduces cost, (b) more directly assess product performance and (c) offer benefits interms of ethical considerations**.**[6] So at early stage of development, cell cultures are usually preferred to whole animal studies. Prediction of *in vivo* absorption based on *in vitro* methodology may help to reduce the volume of essential clinical investgations. As a tool for *in vitro* studies, cell monolayers have been widely used for for evaluating the cellular uptake and cytotoxicity of drug delivery systems. They present many advantages, including easy to culture and studies can be performed within a controlled environment. In many cases a significant correlation between the studies performed on *in vitro* cell monolayers and *in vivo* human studies

has been observed. Hence, *in vitro* studies can be used as predictive tools for estimating the fate and activity of the delivery system in the actual human body.[7] Easy handling, reproducible experimental conditions, and a lack of inter individual variability led to establishment of cell culture models in many labs. Among the numerous techniques available for the prediction of intestinal permeability, the Caco-2 cell line has been extensively used and characterized as a model of the intestinal barrier.[8-12] Caco-2 cell line was established from a moderately well differentiated human colon adenocarcinoma obtained from a 72-year-old patient[13]. Caco-2 cells differentiate spontaneously in culture and exhibit structural and functional differentiation patterns characteristic of mature enterocytes with well established tight junctions and brush border membrane as well as to express several membrane transporters and metabolizing enzymes, allowing the measurement of functional permebility (both passive diffusion and active transport).[14,15] Consequently, this assay is widely accepted by both the pharmaceutical industry and regulatory agencies since the permeability determined using Caco-2 cells correlates well with oral absorption in humans.[16,17] It is necessary to evaluate the cytotoxicity of carrier in drug delivery system. The *In-vitro* cytotoxicity of MSNs was measured by using the MTT assay. MCM-41NPs, MCM-48NPs and SBA-15NPs differ from each other in their specific surface area, pore size, pore wall thickness and shape of nanoparticles. It was reported in many articles that the cytotoxicity of MSNs were dependant on dose, particles physical and chemical property, nanoparticles shape and size as well as depend on type of cell culture used for study.

5.8.1 Principle of MTT Assay

Measurement of cell proliferation and viability forms the basis for numerous in vitro assays of a cell population's response to external factors. The reduction of tetrazolium salts is now widely accepted as a reliable way to examine cell proliferation. MTT assay method was used to measure the cell viability. Basic Principle of MTT assay is related as mitochondrial activity of viable cells which primarily occurs in cytoplasm and also it is rarely occurred in the cell membrane and mitochondria. MTT generally used to measures the mitochondrial dehydrogenate activity into the viable cell. The mitochondrial dehydrogenate activity is exceedingly reliant on the concentration of intracellular NADH In the mitochondrial reduction process, NADH is reduced to NAD+, thus MTT is converted in to formazon.[28-25] It is shown in Fig 5.1 As a consequence of these metabolic processes, the formed

insoluble purple formazan will crystalized and radiate from the cells for a few hours. Only viable cell having the dehydrogenase activity that are able to reduce the significant amount of MTT dye in to formazan.[26] The amount of colour produced is directly proportional to number of viable cells.

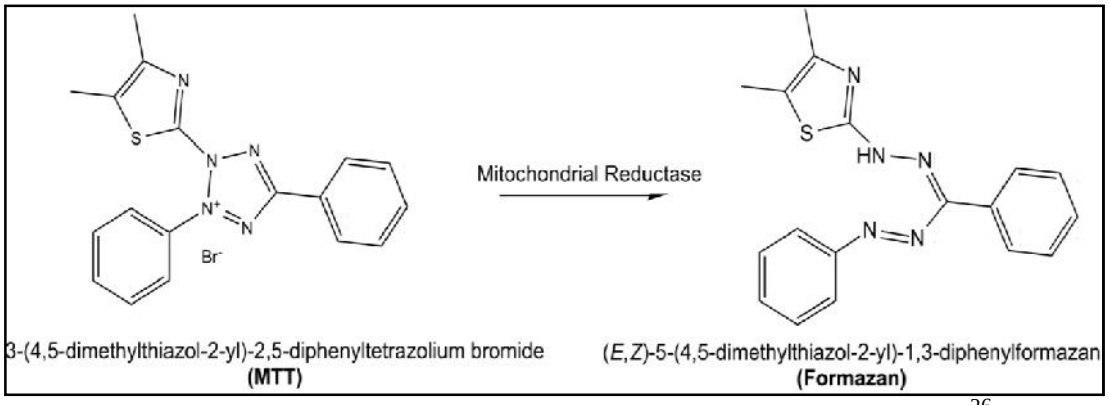

Figure 5.1 Reduction of yellow Tetrazole into purple Formazan[26]

The main objective of this study was to study the effect of morphology of MSNs and surface chemistry as function of incubation time and concentration on caco-2 cells by MTT assay. The selected caco-2 cells were treated with pure drug, MSNs with out drug loaded and R-MSNs prepared formulations. The results show possible cytotoxic effect of MSNs.

5.8.1.1 Cell Culture

Caco-2 cells (NCCS, Pune, India) of passages in between 40-45 were used for in vitro cytotoxicity study experiments. Caco-2 cells were cultured in 25cm2 tissue culture flasks. Dulbecco's MEM medium with 1.5mM/Litre glutamine, 1mM sodium pyruvate, 20% FBS solution, 1%penicillin-streptomycin solution and 1.5gm/Litre of sodium bicarbonate was used as cell culture medium.[27-28] Cells were cultured as a monolayer in an incubator which was set at 37°C in a humidified atmosphere of ~85% relative humidity and ~5% CO2 and medium was replenished every alternate day.

5.8.2 Experiment

Stock solution of MTT (5000µg/ml) was prepared by accurately weighed 50 mg of MTT reagent powder taken in 10ml amber colour volumetric flask and dissolved in 5ml of phosphate buffered saline solution (PBS) and makeup the volume up to 10ml. This prepared MTT stock solution was kept in cool place for the further use.

5.8.2.1 In-vitro cytotoxicity study (MTT assay)

The in-vitro cytotoxicity of all R-MSNs (R-MCM-41NPs, R-MCM-48NPs and R-

SBA-15NPs) and pure RTV was conducted to ascertain their safety for Caco-2 cells using MTT assay. Caco-2 cells were cultured in 96-well plates using DMEM medium supplemented with 20 % FBS solution and 1% Penicillin-streptomycin solution for 24 h at a seeding density of 10000 cells/well. Then the 96 well plates were incubated under a humidified atmosphere of 5 % CO2 at 37 ^{0}C for 24 h. Then the R-MSNs and RTV were dissolved in DMSO and different dilutions were made in DMEM culture medium. The concentration of DMSO was not exceeding more than 0.1% v/v in dilution of solution. After that the culture medium in each of 96 well of each plate was replaced with 100ul of sample solution ranging 10-500ug/ml was added and cells were incubated for 4 h respectively. All four sides of well plate kept empty for blank and few wells were kept untreated with nanoparticles as a negative control. After 6 h of incubation 100 µL of MTT reagent (5mg/mL) was added to each well. After that, the well plates were incubated for additional 3 h at 37°C for cytotoxicity study. Then removed the medium from each plate and replaced it with the 100µl volume of DMSO solvent. Further, the absorbance of each well solution was measured by a micro plate reader at a wavelength of 590 nm. The same procedure was followed for 24 h and 48 h plates. Percentage of cell viability was calculated based on the relative absorbance of MSNs sample treated cells versus cells in the negative control. All calculations, graph preparations and statistical analysis were performed using Microsoft Excel. Percentage of cell viability was calculated based on the absorbance measured relative to the absorbance of cells exposed to the negative control.

5.9 Stability study of R-MSNs

5.9.1 Significance of stability testing

The main objective of stability testing for prepare formulation is to provide any information on how the quality of a drug products or drug substances affected in different environmental factors like light, humidity and temperature with respect to time.

The stability testing process is generally used to determine physical or chemical changes that may affect the efficiency and purity of the drug substances or products. Moreover, stability testing study gives idea and information about storage conditions for drug substances and drug products and it also help for establishment of shelf life and the retest periods for drug substances and drug products.

The mesoporous silica nanoparticles having large surface areas, uniform pore size and having good thermal stability are well reported in literature.[29-34] Also, the drug molecules are easily adsorbed into mesopores and chemically some functional groups of drug molecules may form bonding with silanol group present in MSNs[35] and conversion of drug into amorphous form after loading into MSNs. Hence it is mandatory to check the physical stability of the drug loaded MSNs at accelerated condition.

5.9.2 Method for stability sample preparation and evaluation

Physical stability of drug loaded MSNs was evaluated by performing accelerated stability study: About 200 mg of RTV loaded MSNs (R-MCM-48NPs, R-MCM-41NPs and R-SBA-15NPs) respectively were kept in sealed glass vials and stored for 6 months at temp. 40°C±2°C/75% ± 5% of relative humidity. The samples were withdrawn at established time 1, 3 and 6 month and changes in drug loaded MSNs were observed by DSC and P-XRD instrumental techniques.

Chemical stability of R-MSNs were evaluated by measuring percentage content of RTV in stored formulations by RP-HPLC method.

RESULT AND DISCUSSION

5.10 Synthesis of MCM-41NPs, MCM-48NPs and SBA-15NPs (MSNs)

The synthesized mesoporous silica nanoparticles MCM-48NPs, MCM-41NPs and SBA-15NPs (MSNs) were characterised and evaluated for confirmation of its morphology and structural arrangement by different analytical techniques like powder X-ray diffraction technique, TEM, SEM, FT-IR and N_{2-} adsorption isotherm. The results of characterization of all synthesized MSNs are described below.

5.11 Characterization of MCM-48NPs, MCM-41NPs and SBA-15NPs (MSNs)

5.11.1 SEM and TEM of MSNs

After synthesis of various MSNs; particle size, pore structure and morphology of these synthesized MSNs were confirmed by TEM and SEM analysis respectively. Fig.5.2 A, B and C show the morphology of MCM-48NPs, MCM-41NPs and SBA-15NPs were uniform in shape and having a smooth surface.

Fig 5.2A shows cubic spherical structure of MCM-48NPs and Fig 5.2B and C show hexagonally ordered mesoporous structural arrangement of MCM-41NPs and SBA-15NPs respectively.

Fig 5.3 A, B and C illustrate pore structure and particle size of MCM-48NPs, MCM-41NPs and SBA-15NPs, Fig 5.3A clearly shows the spherical 3D cubic pore network formed by MCM-48NPs, whereas regular 2D hexagonal honeycomb like structure, independent long channel arrangement of MCM-41NPs and SBA-15NPs is shown in Fig 5.3 B and C. Well structured MCM-48NPs show mean particles size around100-200nm while MCM-41NPs and SBA-15NPs have around 200-300nm mean particle size.

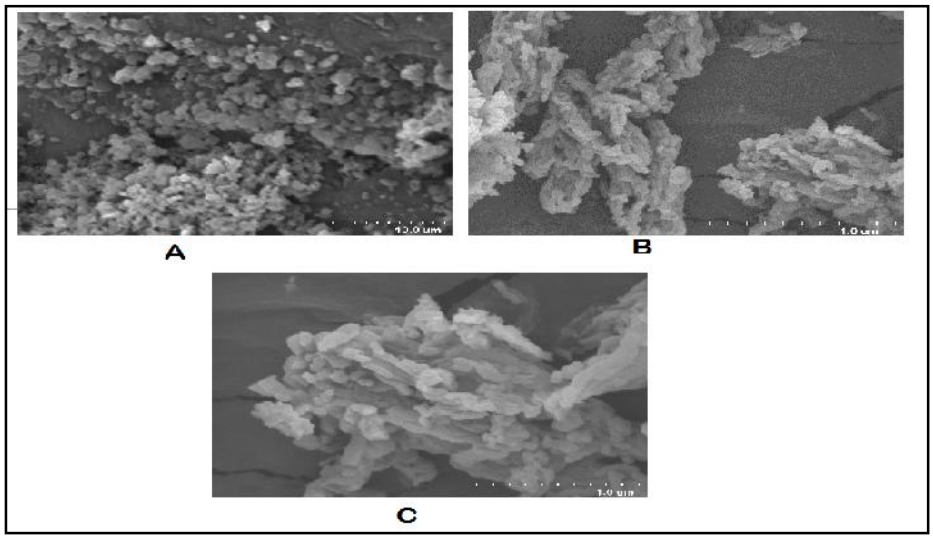

Figure 5.2 SEM images of (A) MCM-48NPs (B) MCM-41NPs and (C) SBA-15NPs

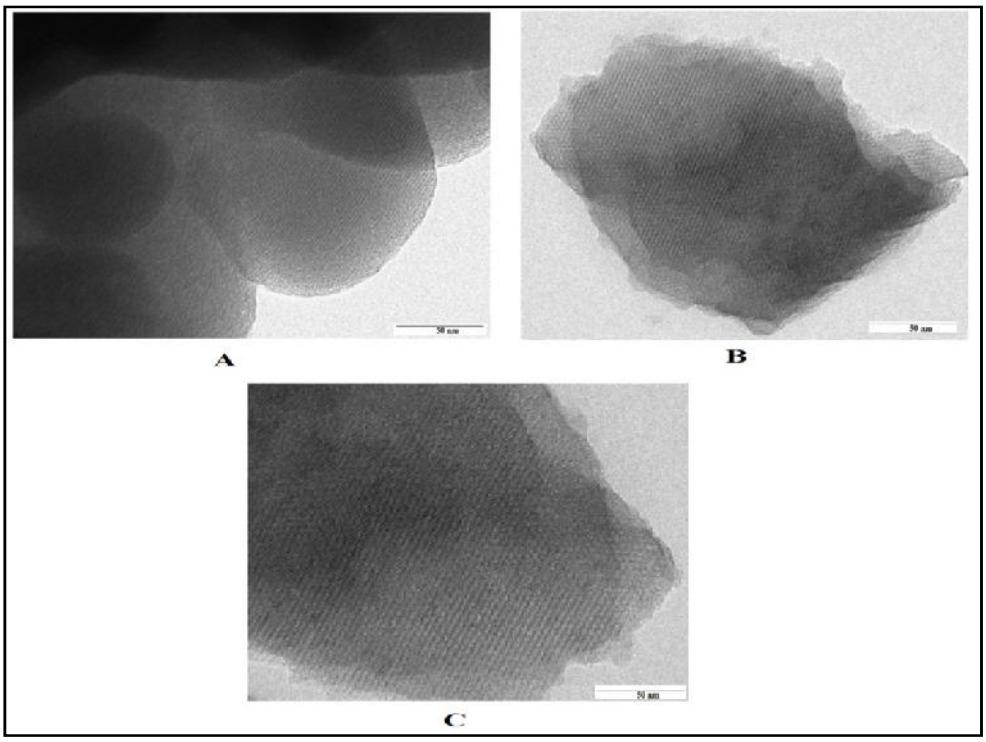

Figure 5.3 TEM images of (A) MCM-48NPs (B) MCM-41NPs and (C) SBA-15NPs

5.11.2 FT-IR of MSNs

The synthesized MSNs were identified using FT-IR study. FT-IR spectra of MCM-48NPs, MCM-41NPs and SBA-15NPs are shown in Fig 5.4 A, B and C respectively. All these FT-IR spectra of MCM-48NPs, MCM-41NPs and SBA-15NPs gave a broad peak between 3350-3500 cm^{-1} which prove the presence of isolated terminal silanol groups. The Si-O-Si and Si-OH stretching vibrations are shown in range 1080-1084 and 805-809 cm^{-1} respectively in all MSNs. The FT-IR spectra of all the synthesized MSNs match with reported standard FT-IR spectra of MCM-48NPs, MCM-41NPs and SBA-15NPs.[36-38]

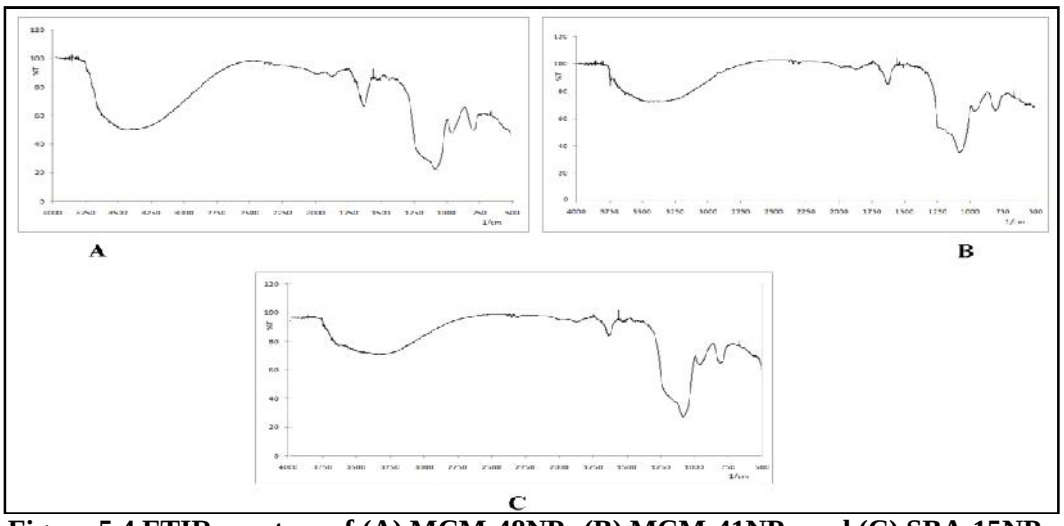

Figure 5.4 FTIR spectras of (A) MCM-48NPs (B) MCM-41NPs and (C) SBA-15NPs

5.11.3 Powder X-ray Diffraction of MSNs

The formation of three MSNs after synthesis was confirmed by PXRD. The samples were scanned at a diffraction angle (2θ) from 1 to 10° in continuous mode at scanning speed of 0.02-2θ/5s[7, 8]. Low angle XRD (L-PXRD) pattern of MCM-48NPs, MCM-41NPs and SBA-15NPs are showing in Fig. 5.5 A, B and C respectively. All the MSNs diffractogram showed their typical diffraction pattern between 1^0-10^0 2θ angle. The L-PXRD pattern of MCM-48NPs shows a strong diffraction peak at 210 and 220, which confirmed the formation of 3D cubic mesostructure with uniform pore channels and it was compliance with reported standard L-PXRD data of MCM-48NPs. Similarly, L-PXRD pattern of MCM-41NPs and SBA-15NPs shows a strong diffraction peak at 100 with two small diffraction peaks at 110 and 200 that confirmed the formation of 2D hexagonal rod-like mesostructure with uniform pore channels. All the synthesized MSNs S-PXRD results show it was in compliance with the reported standard[39-41] L-PXRD pattern of MCM-48NPs, MCM-41NPs and SBA-15NPs.

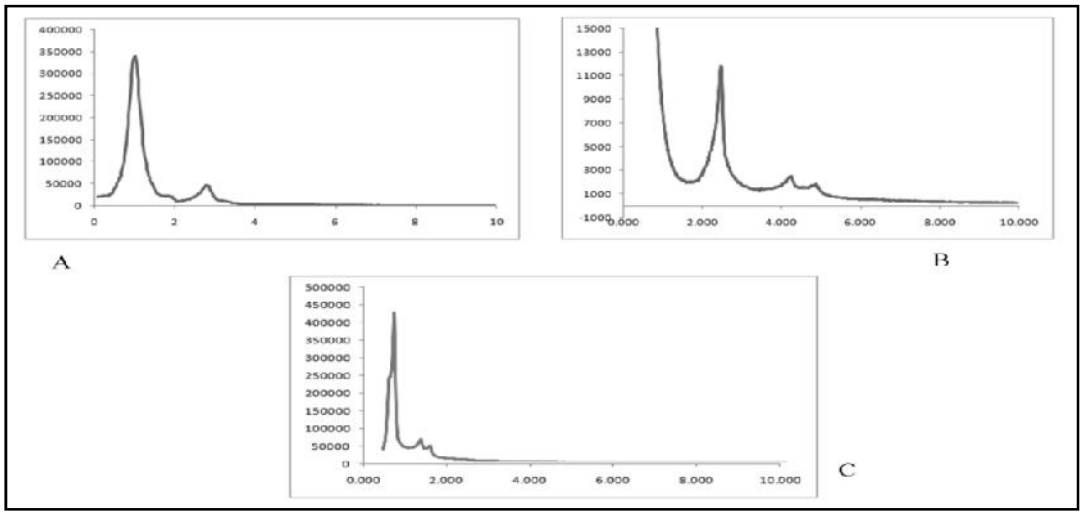

Figure 5.5 L-PXRD (A) MCM-48NPs (B) MCM-41NPs and (C) SBA-15NPs

5.11.4 N2 Adsorption desorption analysis

Before measuring the adsorption-desorption of N_2 in the MSNs, all the MSNs samples were degassed under vaccum at 200°C for 6 h. The inflection of the capillary condensation observed at a P/Po value of about 0.8 for the adsorption isotherms. N_2 adsorption-desorption isotherms and pore size distribution of MCM-48NPs, MCM-41NPs and SBA-15NPs are shown in Fig. 5.6 and 5.7 respectively. All the N_2 adsorption-desorption isotherms showed typical type IV isotherms and hysteresis loop (according to IUPAC) which confirmed that all the developed MSNs

have mesoporous property. The isotherms of all MSNs show a hysteresis loop at high relative pressure, which has been assigned to the presence of interparticle porosity[42]. The calculated BET specific surface area for MCM-48NPs, MCM-41NPs and SBA-15NPs was 1220.29m²/g, 935.76m²/g and 880.66m²/g respectively. The mesopores volume for MCM-48NPs, MCM-41NPs and SBA-15NPs was found to be 0.96cm3/g, 0.82cm3/g and 0.89 cm3/g nm and average pore size was 3.2nm, 3.9nm and 5.9nm respectively. The numerical data of BET specific surface area, pore volume and size for all MSNs are shown in Table 5.2

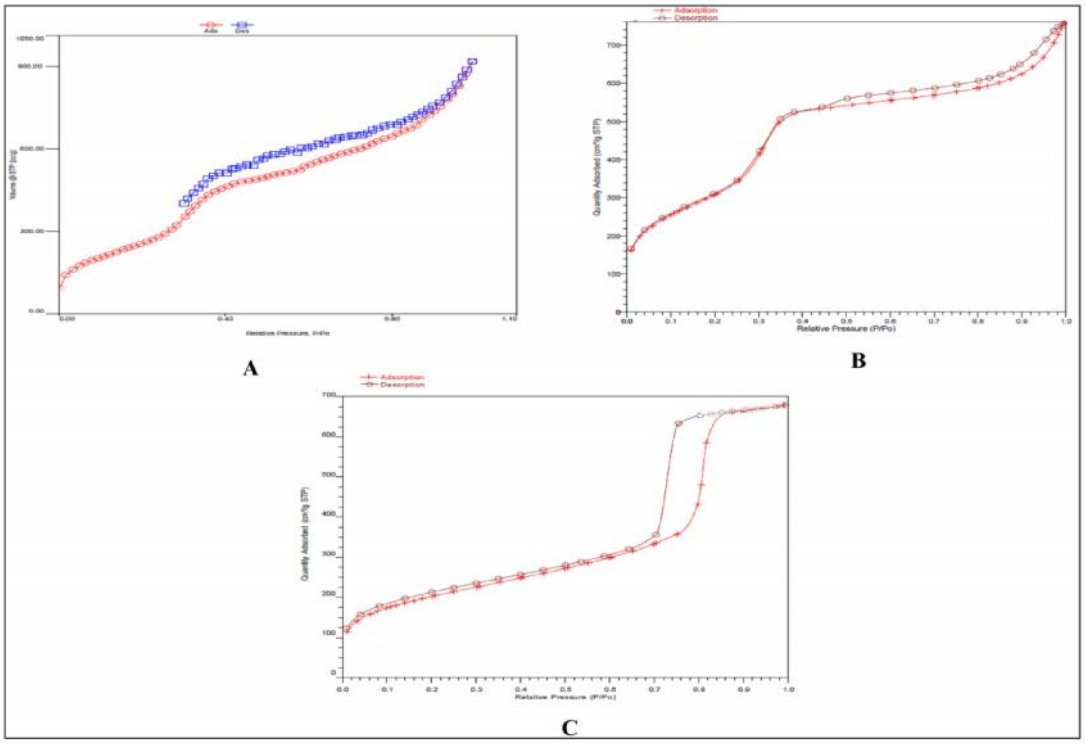

Figure 5.6 N2 Adsorption desorption of (A) MCM-48NPs (B) MCM-41NPs and (C) SBA-15NPs

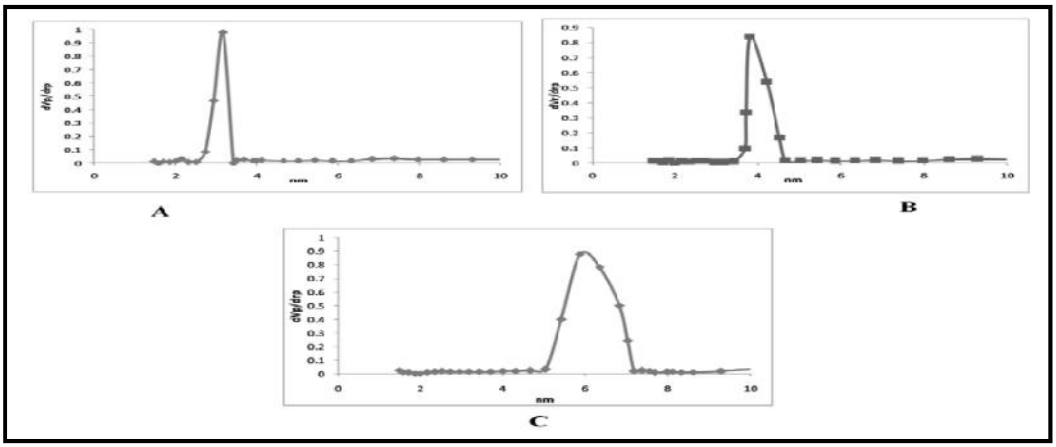

Figure 5.7 Pore size graph of (A) MCM-48NPs (B) MCM-41NPs and (C) SBA-15NPs

Table 5.2 BET surface area, pore volume and pore diameter of MSNs

MSNs	SBET (m^2/g)	Pore volume (cm^3/g)	Pore diameter (nm)	SEM Analysis
MCM-48NPs	1220.29	0.96	3.2	spherical
MCM-41NPs	935.76	0.82	3.9	Hexagonal
SBA-15NPs	880.66	0.89	5.9	Hexagonal

The analytical study confirmed the formation of mesoporous silica nanoparticles MCM-41NPs, MCM-48NPs and SBA-15NPs (MSNs). Their unique properties are show in Table 5.2.

5.12 RTV loading in Mesoporous Silica Nanoparticles (MSNs)

The drug loading into the MSNs is also controlled by the chemical nature of the pores and shape and size of the nanoparticles. The inorganic networks of MSNs have plenty of silanol groups (Si-OH), present into/on the mesopores surface (Fig 5.8) that would interact with the functional groups of the drugs through hydrogen bond.[45,46] Attracting interaction between the silanol group of MSNs and functional group of the drug, the drug molecules either confined within the pores or they adsorbed to the surface of MSNs

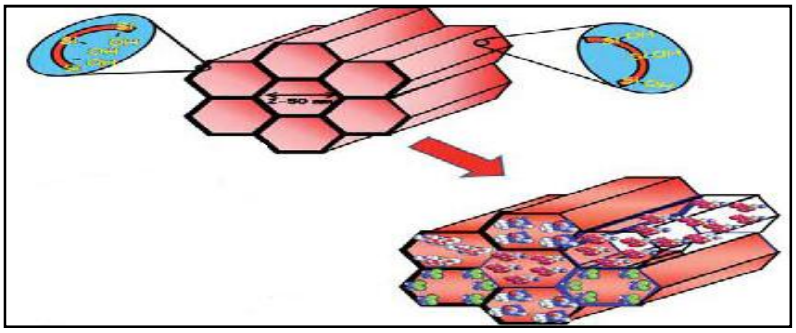

Figure 5.8 Graphical representation of textural properties and drug loading in MSNs[47]

The probable mechanism of drug loading is that, the a C=O group of amide and oxygen of ester group of RTV would form hydrogen bonds with the silanol groups (Fig 5.9) of developed mesoporous silica nanoparticles and consequently drug molecules would be retained into the mesopores.[45,46]

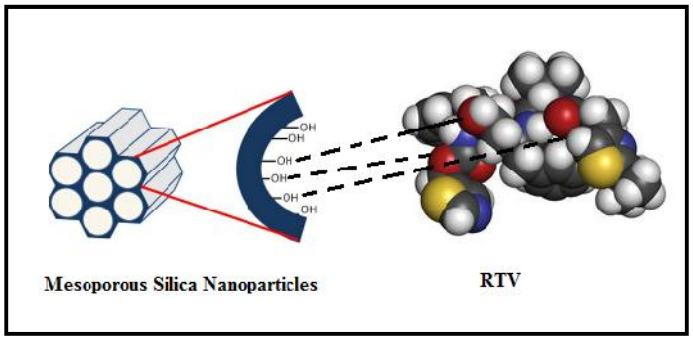

Figure 5.9 Graphical representation of RTV linkage to silanol group of MSNs[48]

5.13 Optimization of drug loading procedure

The drug loading process was optimized by selecting proper ratio of drug to carrier (MSNs).

5.13.1 Ratio of drug to carrier

Ratio of drug as to MSNs carrier greatly affects the loading efficiency. It was necessary to find out optimum drug to MSNs carrier ratio. To optimize the ratio of drug to carrier, different proportions of MSNs to drug were taken. Fig. 5.10, 5.11 and 5.12 shows DSC thermogram of different drug: carrier ratio and also confirm the drug loaded in different MSNs by DSC. The amount of drug entrapped in different MSNs with different carrier ratio was calculated with the help of the calibration curve obtained by UV spectroscopy.

Factors like different solvents (like acetonitrile, mixture of acetonitrile and methanol) and stirring rate and time did not affect the % loading efficiency of RTV in all mesoporous silica nanoparticles.

The % entrapment efficiency of drug and % loading efficiency for MSNs were calculated by using equation 1 and 2 respectively

$$\% \text{ Entrapment efficiency} = \frac{\text{Weight of RTV in nanoparticles}}{\text{Weight of drug initially added}} * 100 \quad \text{------ (1)}$$

$$\% \text{ Loading Efficiency} = \frac{\text{weight of RTV in nanoparticles}}{\text{Total weight of sample}} * 100 \quad \text{------- (2)}$$

Ratio was optimized by taking fixed proportion of RTV and different proportion of MSNs respectively. Four different drugs: MSNs proportions were tested i.e. 1:1, 1:1.25, 1:1.5 and 1:2. It was found that maximum drug loading was achieved with 1:1.5 drug: carrier ratio and % entrapment efficiency of RTV in MCM-48NPs was 98.33, in MCM-41NPs it was 84.26 % and in SBA-15NPs it was 99.52% respectively. The results of drug loading procedure are shown in table 5.3

Table 5.3 Effects of drug: MSNs ratio on drug loading

Weight ratio Drug: Carrier	% Drug loading in MCM-48NPs	% Drug loading in MCM-41NPs	% Drug loading in SBA-15NPs	DSC results	Remarks
1:1	-	-	-	Sharp fusion peak of RTV was observed	RTV not totally entrapped in all MSNs

1:1.25	-	-	-	Sharp fusion peak of RTV was observed	RTV not totally entrapped in all MSNs
1:1.5	44.12%	37.45%	52.36%	No fusion peak of RTV was observed	RTV was totally entrapped in all MSNs
1:2	40.89%	32.76%	47.42%	No fusion peak of RTV was observed	RTV was totally entrapped in all MSNs

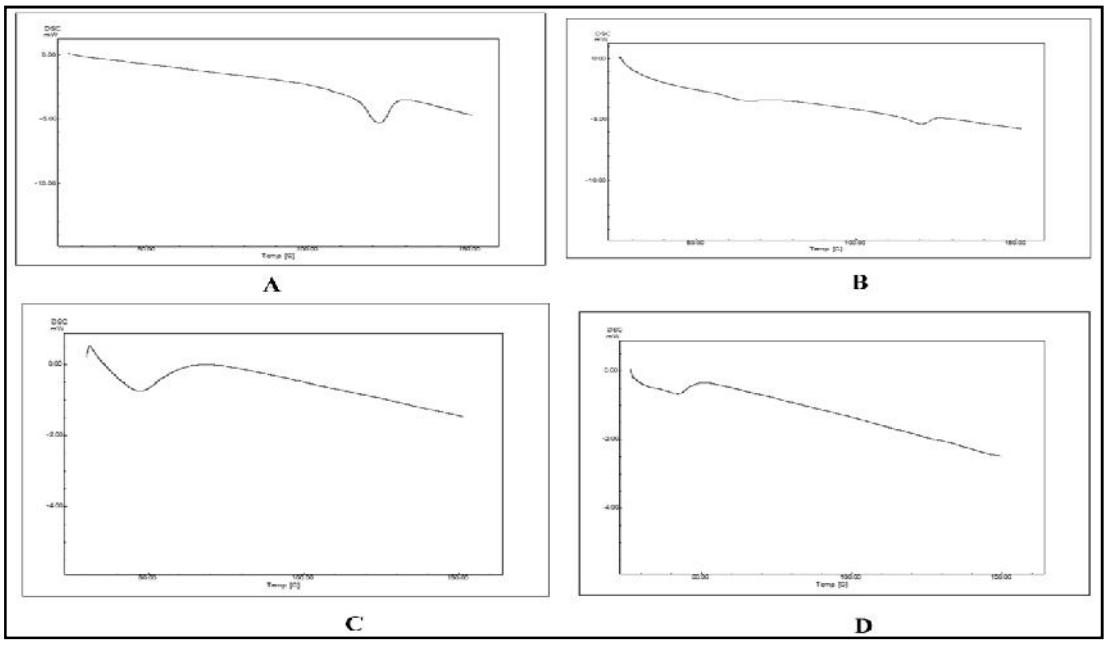

Figure 5.10 DSC thermogram of optimization of RTV loading in MCM-48NPs RTV: MCM-48NPs (A) 1:1 (B) 1:1.25 (C) 1:1.5 and (D) 1:2

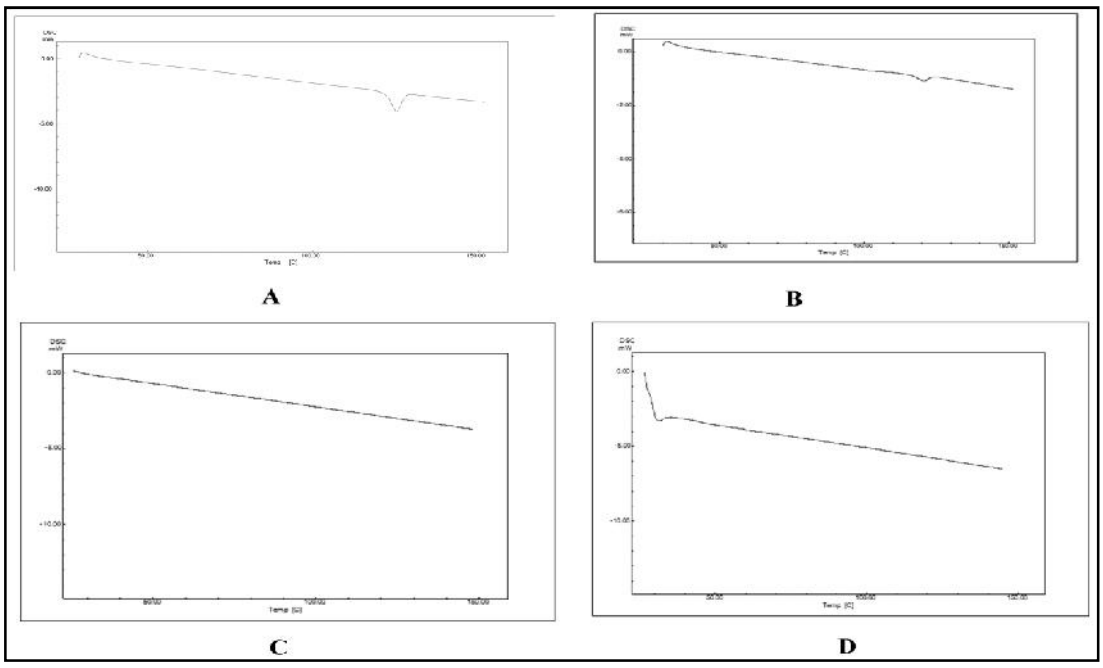

Figure 5.11 DSC thermogram of optimization of RTV loading in MCM-41NPs RTV: MCM-41NPs (A) 1:1 (B) 1:1.25 (C) 1:1.5 and (D) 1:2

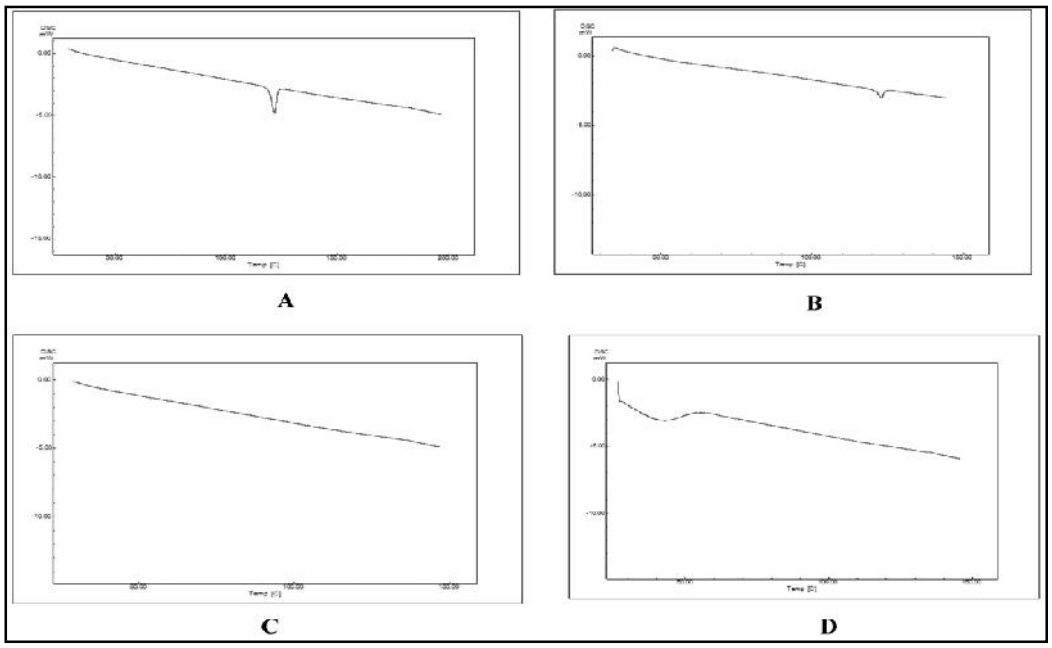

Figure 5.12 DSC thermogram of optimization of RTV loading in SBA-15NPs RTV: SBA-15NPs (A) 1:1 (B) 1:1.25 (C) 1:1.5 and (D) 1:2

5.13.2 Thermogravimetric Analysis

TGA thermograms were obtained to evaluate and further confirm the loading (wt %) of the RTV in MCM-48NPs, MCM-41NPs and SBA-15NPs. In Fig 5.13, TGA thermogram of RTV, R-MCM-48NPs, R-MCM-41NPs and R-SBA-15NPs show their stepwise weight loss. The thermogram in Fig. 5.13 A show that RTV remain unchanged until the temperature of analysis reaches 200°C. Then there was a gradual weight loss between 200 to 290°C and a second step between 310 and 420°C due to ultimate RTV decomposition. Fig. 5.13 C, R-MCM-48NPs shows thermal behaviour of initial gradual reduction in weight between 170° and 270°C that was attributed to initial drug loss and a second gradual reduction between 290 and 420°C due to final RTV decomposition. The stable line in thermogram after 420°C is because only silica nanoparticles were remained. Based on the %weight loss, the loading capacity of MCM-48NPs was determined to be 45%. The same weight loss pattern were found for RTV loaded MCM-41NPs and SBA-15NPs respectively in Fig 5.13 B and D, but it shows different loading capacity of RTV and it was 38% and 53% respectively on the basis of % weight loss of RTV. Therefore TGA and UV spectroscopy showed almost similar results of RTV loading in different carrier and results shown in table 5.4

Table 5.4 Drug loading efficiency results for R-MSNs by two different Method

Drug loading (% loading)	UV Method	TGA Method
MCM-48	43.23%	45%
MCM-41	37.12%	38%
SBA-15	50.34%	53%

MCM-48NPs have high loading efficiency than the MCM-41NPs mainly due to their large surface area and large pore volume due to this it adsorbed the large quantity of drug molecules. Likely the SBA-15 NPs and MCM-41NPs almost have the same surface area and pore volume but due to large pore size and having large number of silanol group present on the surface; due to this it have high loading efficiency. After confirming the RTV was loaded in MCM-48NPs, MCM-41NPs and SBA-15NPs, it were designated as R-MCM-48NPs, R-MCM-41NPs and R-SBA-15NPs.

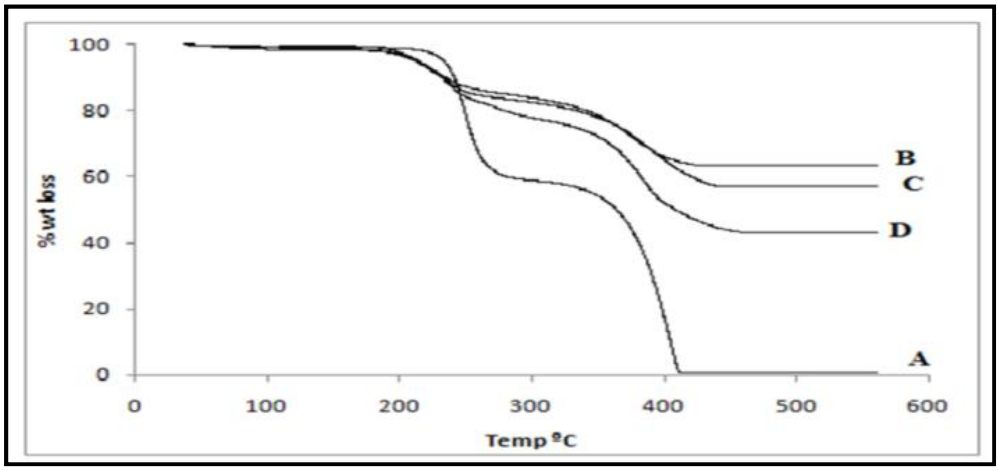

Figure 5.13 TGA Thermogram of (A) RTV (B) R-MCM-41NPs (C) R-MCM-48NPs and (D) R-SBA-15NPs

5.14 Characterization and Evaluation of R-MCM-48NPs, R-MCM-41NPs and R-SBA-15NPs (R-MSNs)

Drug loaded R-MCM-48NPs, R-MCM-41NPs and R-SBA-15NPs (R-MSNs) were characterized and evaluated for their intact mesoporous nature of nanoparticles and also maximum drug loading. Different instrumental techniques like TEM, FTIR, DSC, P-XRD and N2 adsorption desorption were used.

5.14.1 Transmission electron microscopy (TEM)

The R-MSNs samples were analyzed by TEM. The TEM images confirmed that, mesoporous structure of MCM-48NPs, MCM-41NPs and SBA-15NPs was as such after drug loading (Fig 5.14 A, B and C respectively). Dark spots in TEM image of R-MSNs confirmed the presence of RTV molecules in the mesopores.

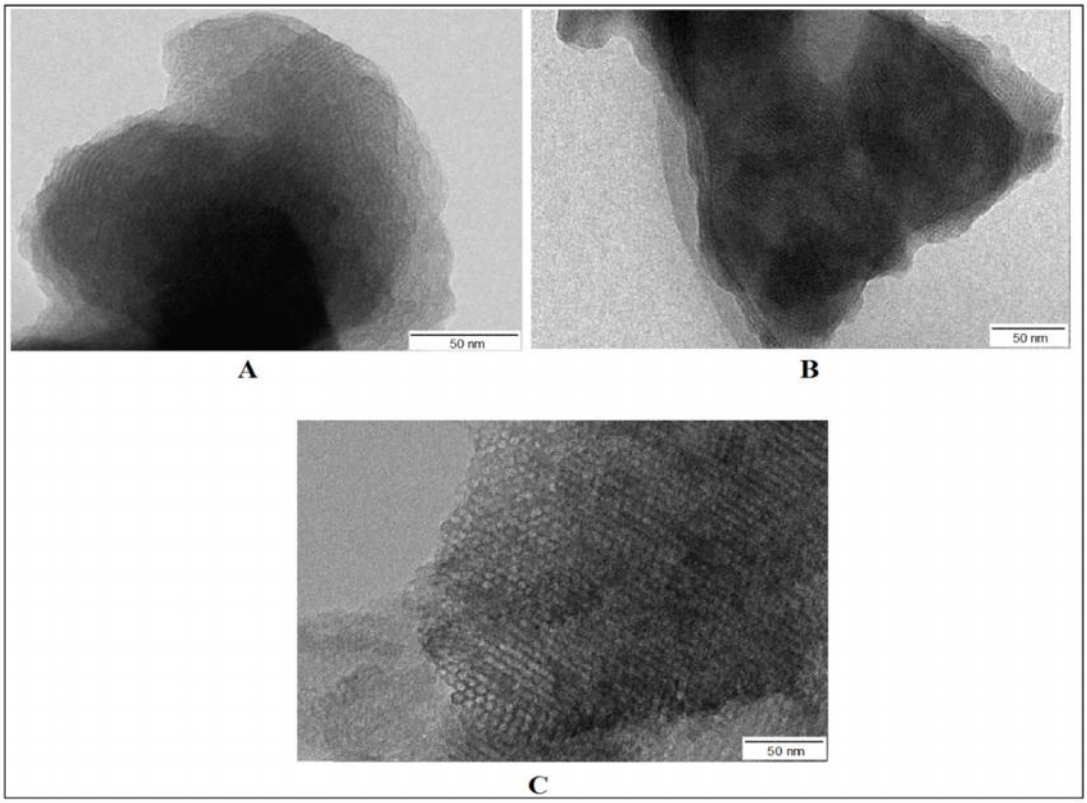

Figure 5.14 TEM images after RTV loading in (A) MCM-48NPs (B) MCM-41NPs and (C) SBA-15NPs

5.14.2 FTIR analysis

For functional group identification and confirming the compatibility between RTV and silica nanoparticles, FT-IR study was carried out. FT-IR spectra of pure RTV is shown in Fig. 5.15. The RTV spectrum shows peaks at 3327 cm-1 relative to the N-H stretching of an amide group, 2962 cm-1 relative to hydrogen-bonded acid within the molecule, 1706 cm-1 relative to the ester group, 1660, 1611 and 1540 cm-1 relative to –C═C– stretching aromatic carbons. The FT-IR spectrum of MCM-48NPs, MCM-41NPs and SBA-15NPs (Fig.5.4 A, B and C) show a broad peak between 3350-3500 cm-1 which indicating the presence of isolated terminal silanol groups. The Si-O-Si and Si-OH stretching vibrations are shown at 1084 and 801 cm-1 respectively. In Fig 5.16A, R-MCM-48NPs-PM spectrum show characteristic peaks of RTV and MCM-48NPs which proves compatibility between both drug and silica nanoparticles. Similar results were obtained for R-MCM-41NPs-PM and R-SBA-15NPs-PM and are shown in Fig.5.16 B and C. On the other hand, in Fig.5.17 A, B and C, R-MCM-48NPs, R-MCM-41NPs and R-SBA-15NPs spectra show a remarkable decrease of the peak

at 2962 cm-1, 1706 cm-1 and slight shifting of –C═C– stretching aromatic carbons with the disappearance of other major peaks of RTV, indicating the complete uptake of the RTV by mesoporous silica nanoparticles. These changes also suggested that the isolated terminal silanol group present in mesoporous silica nanoparticles have some interactions with RTV functional groups.

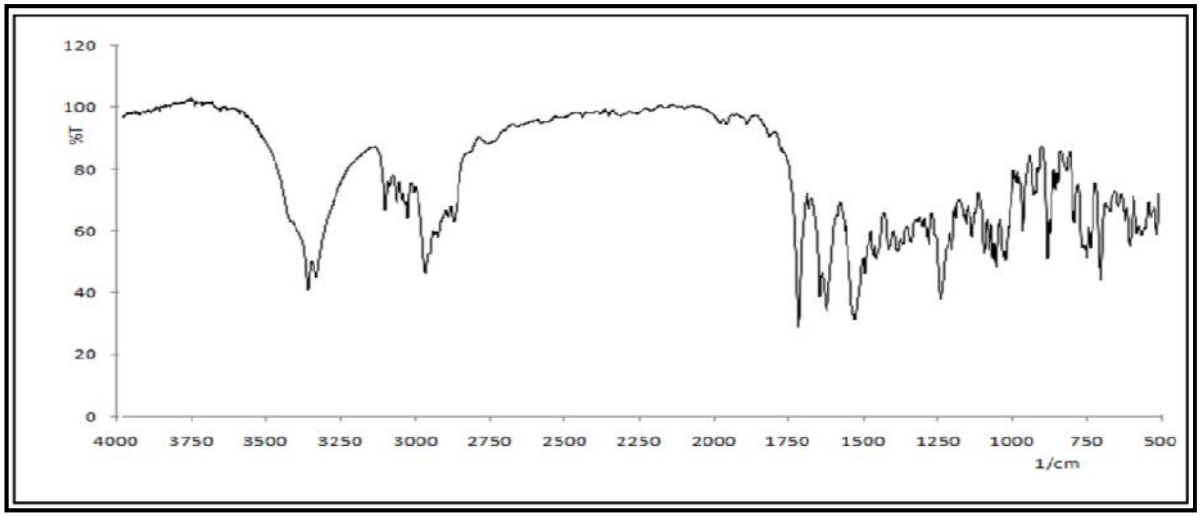

Figure 5.15 FT-IR spectra of RTV

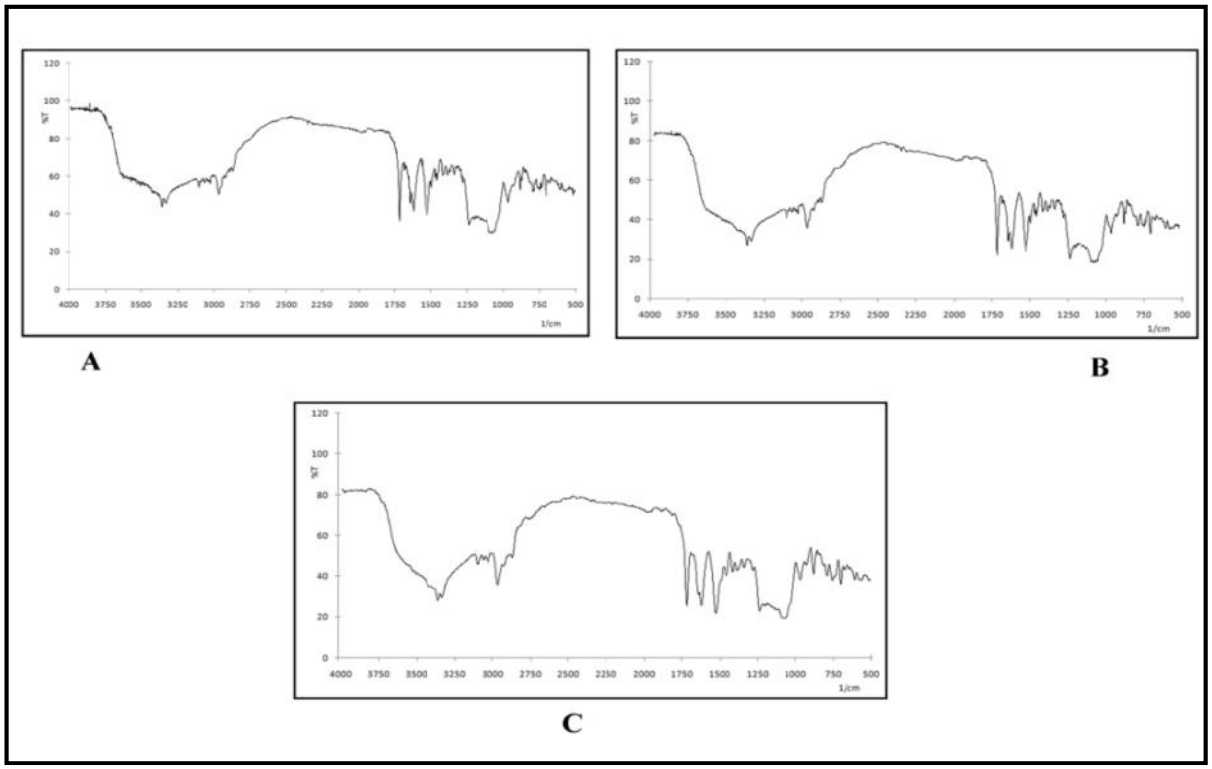

Figure 5.16 FT-IR spectra of physical Mixture of (A) RTV+MCM-48NPs (B) RTV+MCM-41NPs and (C) RTV+SBA-15NPs

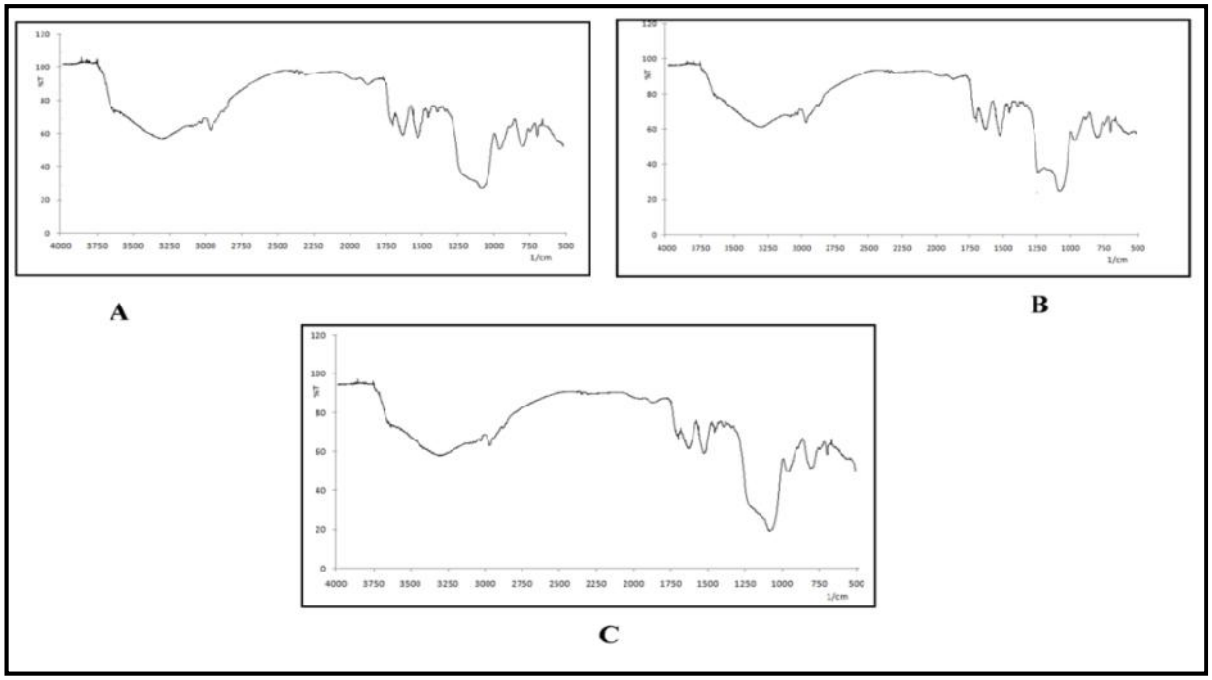

Figure 5.17 FT-IR spectra of (A) R-MCM-48NPs (B) R-MCM-41NPs and (C) R-SBA-15NPs

5.14.3 Differential Scanning Calorimetry (DSC)

The DSC thermogram of crystalline pure RTV, MCM-48NPs, physical mixture of RTV and MCM-48 and R-MCM-48NPs are shown in Fig.5.18 Crystalline RTV thermogram exhibited a sharp endothermic peak at 123°C which corresponds to its fusion temperature point (Fig. 5.18 A(A). MCM-48NPs thermogram did not show any transition because the fusion point of silica is very high (Fig. 5.18 A(B). In physical mixtures, the sharp endothermic peak of RTV was present indicating the compatibility between MSNs and pure RTV (Fig. 5.18 A(C). In Fig 5.18 A(D) The R-MCM-48NPs thermogram did not show any sharp endothermic peak of RTV. The same results were found for MCM-41, R-MCM-41NPs-PM, R-MCM-41NPs and SBA-15, R-SBA-15NPs-PM, R-SBA-15NPs in Fig 5.18 B and 5.18 C.

All results suggested that no RTV was present on the outer surface of all MSNs (Fig. 5.18) that confirmed successful loading of RTV in nanoparticles.

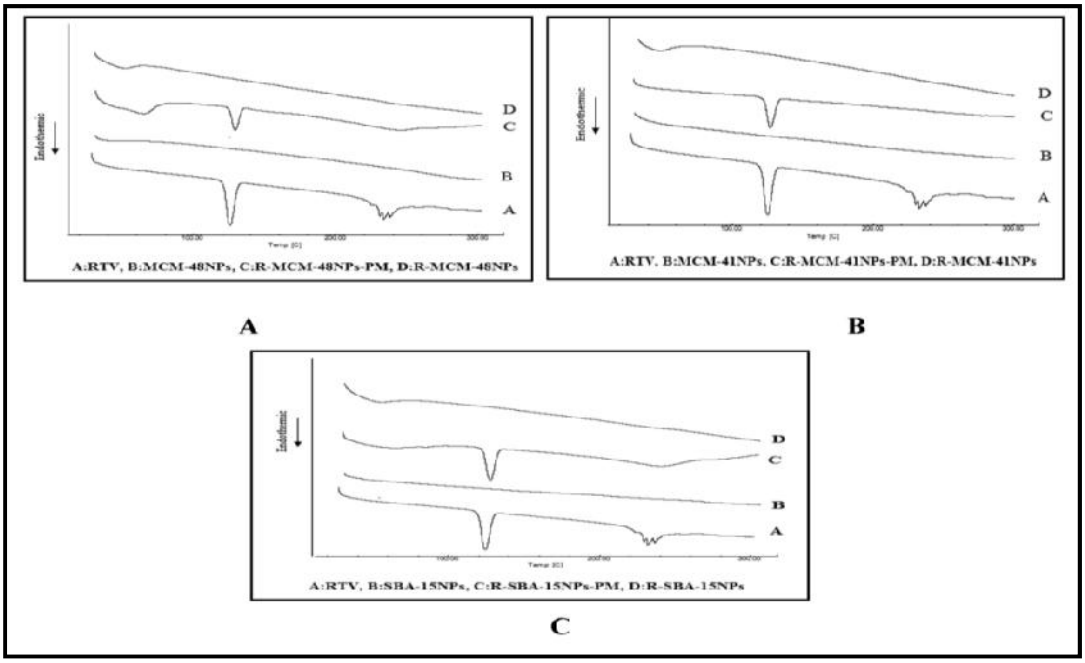

Figure 5.18 DSC thermogram of (A) MCM-48NPs (B) MCM-41NPs and (C) SBA-15NPs

5.14.4 Powder X-ray diffraction (XRD)

The intactness of mesopores structure of the MCM-48NPs, MCM-41NPs and SBA-15NPs after RTV loading was confirmed by S-PXRD. S-PXRD patterns were studied after the loading process. Before RTV loading MCM-48NPs, MCM-41NPs and SBA-15NPs diffractogram showed typical reflections pattern between 0.5° to10° that was shown in Fig 5.5 A, B and C. The same diffraction patterns with decreased intensity of peaks in MCM-48NPs, MCM-41NPs and SBA-15NPs were observed in Fig 5.19 A, B and C, after RTV loading, confirming that the mesoporous structure was intact after drug loading. The wide angle P-XRD pattern of pure RTV and R-MCM-48NPs, R-MCM-41NPs and R-SBA-15NPs are shown in Fig 5.20 a, b, c and d. The wide angle powder XRD pattern of pure RTV showed several characteristic peaks at region 5-40° in the 2θ/5s region, which confirmed the crystalline nature of the RTV. The R-MCM-48NPs, R-MCM-41NPs and R-SBA-15NPs did not show these characteristic peaks in W-PXRD pattern confirming that the RTV was completely loaded in nanoparticles and no crystalline drug remained on the outer surface of nanoparticles respectively.

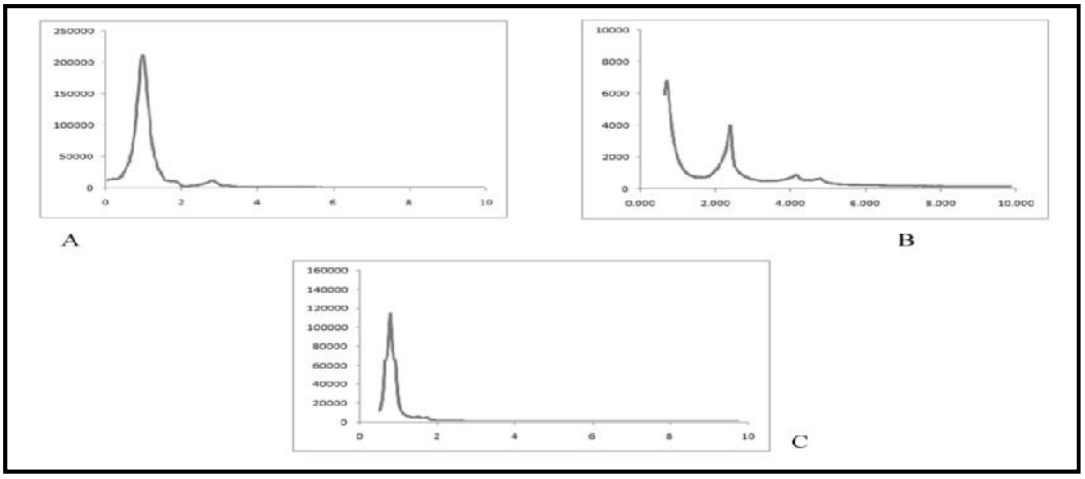

Figure 5.19 S-PXRD (A) R-MCM-48NPs, (B) R-MCM-41NPs and (C) R-SBA-15NPs

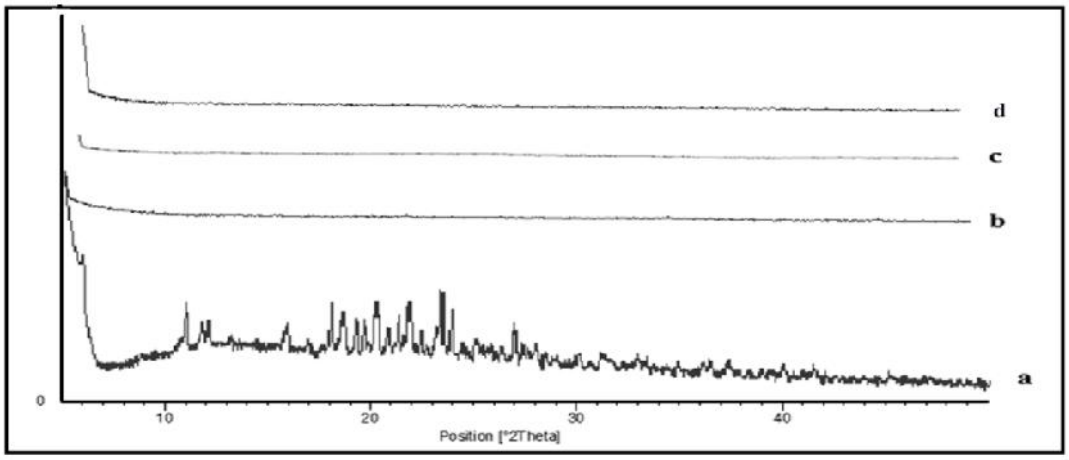

Figure 5.20 W-PXRD (A) R-MCM-48NPs, (B) R-MCM-41NPs and (C) R-SBA-15NPs

5.14.5 Nitrogen adsorption isotherm (BET surface analysis)

After the confirmation of the integrity of the mesostructure, next important point was to check whether the drug molecules are confined inside the mesopores or they are just on the outer surface of the MSNs. Nitrogen adsorption analysis was performed to find out the status of drug molecules. The nitrogen adsorption isotherms were obtained for the pore size distribution and the pore volume determination of MSNs, before and after the loading process.

The pore volume and surface area are normally decreased as a consequence of the MSNs–drug interaction. It can be noted from Fig. 5.21 and 5.22 that the available pore volume was decreased after the drug loading. Decrease in pore volume suggested that the drug molecules are partially filling the mesopores, i.e. the drug molecules are being confined inside the pores.

All the isotherm of MCM-48NPs, MCM-41NPs and SBA-15NPs shows typical type IV isotherm according to IUPAC classification represents the mesoporosity. The isotherm recorded for MCM-48NPs, MCM-41NPs and SBA-15NPs also shows a hysteresis loop at high relative pressure, which has been ascribed to the presence of interparticle porosity.

The calculated BET specific surface area for MCM-48NPs, MCM-41NPs and SBA-15NPs were found to be 1220.29, 935.76 and 880.66m^2/g respectively and after RTV loading in to MCM-48NPs, MCM-41NPs and SBA-15NPs BET surface area were found to be 440.60, 380.15 and 243.90m^2/g respectively. The adsorption isotherms of RTV loaded MCM-48NPs, MCM-41NPs and SBA-15NPs showed that the adsorbed nitrogen volume decreased after drug loading. Correspondingly, the average pore size distribution for RTV loaded MCM-48NPs, MCM-41NPs and SBA-15NPs calculated by the BJH–KJS method, was shifted from 3.20 nm to 2.71 nm for R-MCM-48NPs, 3.92nm to 3.43nm for R-MCM-41NPs and 5.94nm to 5.43nm for R-SBA-15NPs. The mesopore volume also decreased from 0.96 cm^3/g to 0.31 cm^3/g nm for R-MCM-48NPs, 0.82cm^3/g to 0.46cm^3/g for R-MCM-41NPs and 0.89cm^3/g to 0.27 cm^3/g for R-SBA-15NPs (Fig 5.22 A, B and C). Numerical data are shown in Table 5.5 for MCM-48NPs, MCM-41NPs and SBA-15NPs and R-MCM-48NPs, R-MCM-41NPs and R-SBA-15NPs.

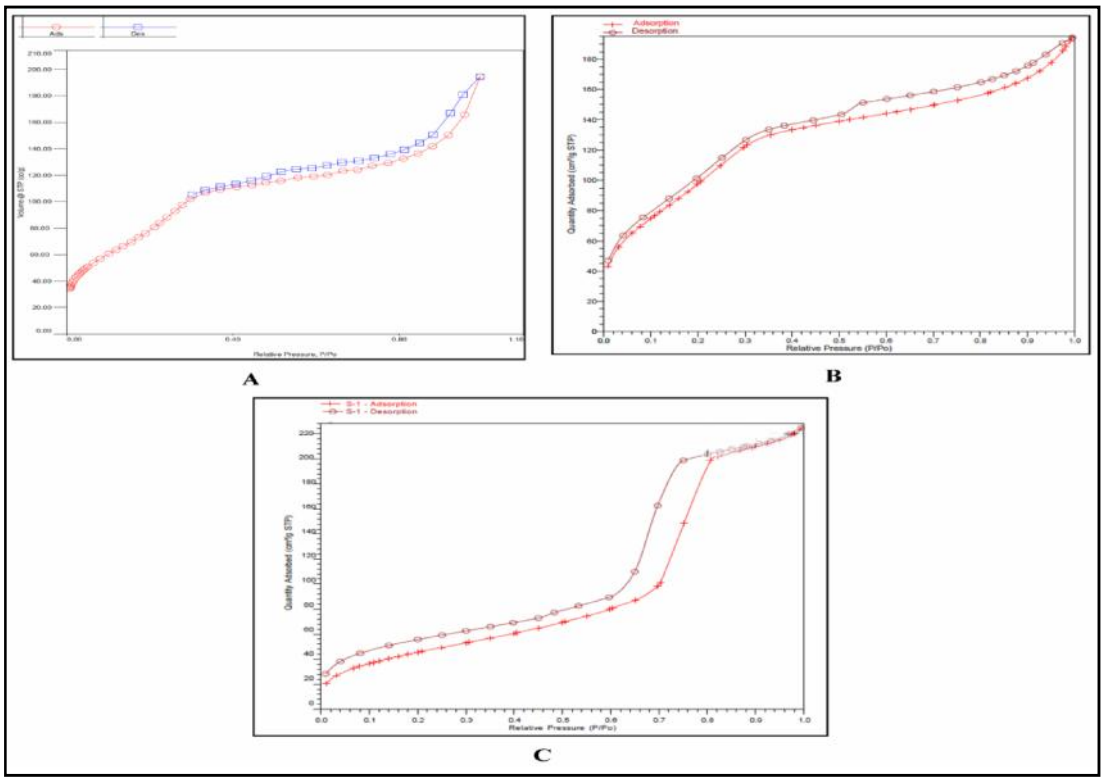

Figure 5.21 N2 adsorption desorption isotherms of (A) R-MCM-48NPs, (B) R-MCM-41NPs and (C) R-SBA-15NPs

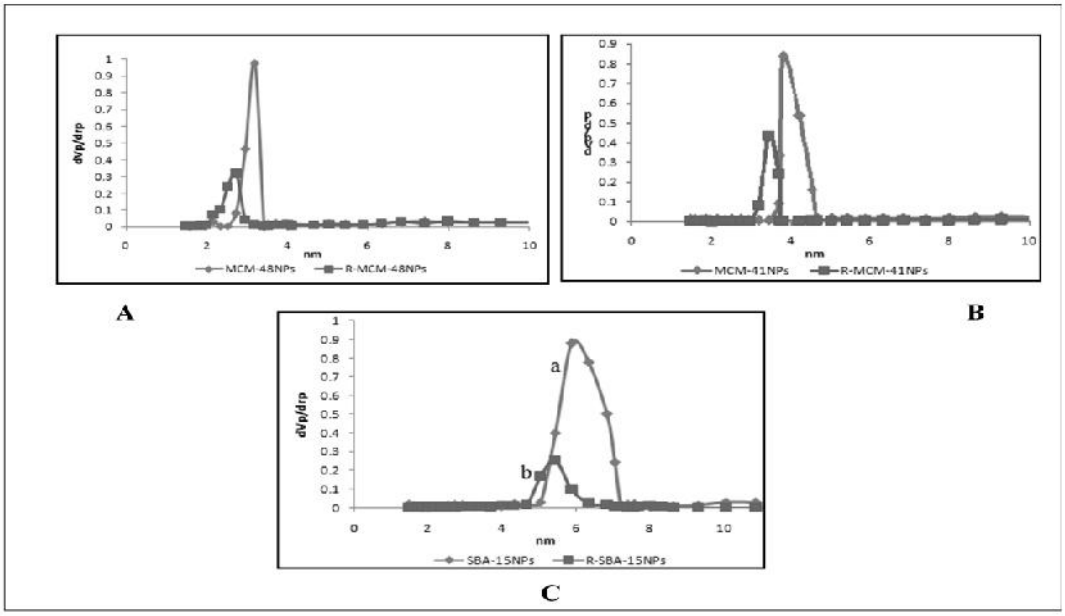

Figure 5.22 Pore size after RTV loading in (A) MCM-48NPs, (B) MCM-41NPs and (C) SBA-15NPs

Table 5.5 BET surface area Pore diameter and volume of MCM-48NPs, MCM-41NPs and SBA-15NPs before and after RTV loading

Name of compound	BET surface area	Pore volume	Pore diameter
MCM-48NPs	1220.29 m^2/g	0.96cm^3/g	3.2nm
R-MCM-48NPs	440.60 m^2/g	0.31cm3/g	2.7nm
MCM-41NPs	935.76 m^2/g	0.82cm^3/g	3.9nm
R-MCM-41NPs	380.15 m^2/g	0.46cm3/g	3.3nm
SBA-15NPs	880.66 m^2/g	0.89cm^3/g	5.9nm
R-SBA-15NPs	243.90 m^2/g	0.27cm^3/g	5.4nm

5.15 Tablet Formulations of R-MCM-48NPs, R-MCM-41NPs and R-SBA-15NPs (R-MSNs-NPs)

Ritonavir (100 mg) tablets were prepared using R-MSNs by same procedure and using excipients which are mention in section 5.5. Prepared tablets were characterized by various parameters such as weight variation, hardness, friability and disintegration time etc and results are shown in table 5.6

Table 5.6 Evaluation of Prepared R-MCM-41NPs and R-MCM-48NPs Tablets

Parameters	R-MCM-48NPs	R-MCM-41NPs	R-SBA-15NPs
Hardness kP	6-8 kP	6-8 kP	6-8 kP
Friability (%)	< 1 %	< 1 %	< 1 %
Disintegration time (Min)	1±0.2 min	2±0.3 min	1±0.2 min
Weight variation (mg)	503.62 ±6.88	498.35 ±5.88	505.62 ±7.38
Drug content (%)	98.12-101.56%	98.55-100.56%	99.12-100.36%

MF for ritonavir is available as film coated tablet with having 100mg of RTV.

5.16 In-vitro dissolution study

PLE is used as surfactant in dissolution medium and as per FDA minimum amount of surfactant can be use for the dissolution study as per requirement in developed formulation. Therefore dissolution tests were performed at different pH conditions with using minimum amount of surfactant at a particular pH in order to investigate the drug release behavior in different regions of gastrointestinal tract. RTV dissolution from different MSNs was compared with those from pure crystalline RTV and MF. Drug release studies were performed to see the release pattern of pure RTV and drug loaded mesoporous silica nanoparticles in 0.1 N HCl, pH 4.5 acetate buffer with 0.75% PLE and pH 6.8 phosphate buffer with 0.75% PLE. The dissolution rate was significantly enhanced in the R-MCM-48NPs, R-MCM-41NPs and R-SBA-15NPs (R-MSNs) as compared to pure RTV. The augment in dissolution rate in silica nanoparticles was observed due to the conversion of RTV into amorphous form after loading into mesoporous nanoparticles. The RTV release profiles of R-MCM-48NP and R-SBA-15NPs showed more than 95% drug release in all dissolution media within 45 min, whereas R-MCM-41NP showed almost 72%, 59.9% and 53% drug release in 0.1 N HCl, pH 4.5 acetate buffer with 0.75% PLE and pH 6.8 phosphate buffer with 0.75% PLE respectively. Pure RTV and RTV MF did not achieve complete dissolution in any of the selected media over the test period of 60 min. The enhancement in dissolution rate can be attributed to the fact that RTV may be in amorphous form after incorporation in mesopores of nanoparticles[49-52] that improves the solubility rate and dissolution of RTV. In dissolution profile of RTV, MCM-48NPs show better dissolution profile than R-MCM-41NPs may be due to the high surface area and small pore size of nanoparticles. Because of high surface area it adsorbs more drug molecule very efficiently. The 3D interconnected MCM-48NPs cubic spherical shape nanoparticles gave faster dissolution and more rapid diffusion in the dissolution medium while, MCM-41NPs has 2D hexagonally ordered mesoporous structural arrangement, appeared to prevent the drug molecules in the pore channels from diffusing into the dissolution medium resulting slow drug release.[53,54] R-SBA-15NPs also shows more than 90% dissolution of RTV in all dissolution media, which may be due to high amount of silanol group present[55] in SBA-15NPs that can adsorb more amount of RTV molecules and also SI-OH groups on SBA-15NPs form very weak bonding with RTV molecules as compared to MCM-41NPs, that can be easily and quickly broken down in dissolution media.

Because of all these reasons SBA-15NPs gave rapid dissolution as well as more diffusion in the dissolution medium. The graphical representation of release profile of RTV from pure RTV, develop formulation of RTV with various mesoporous silica nanoparticles and MF in different dissolution media are shown in Fig 5.23. While comparing dissolution rate from R-SBA-15NPs and R-MCM 48NPS, it was almost similar with slight faster drug release from R-SBA-15.

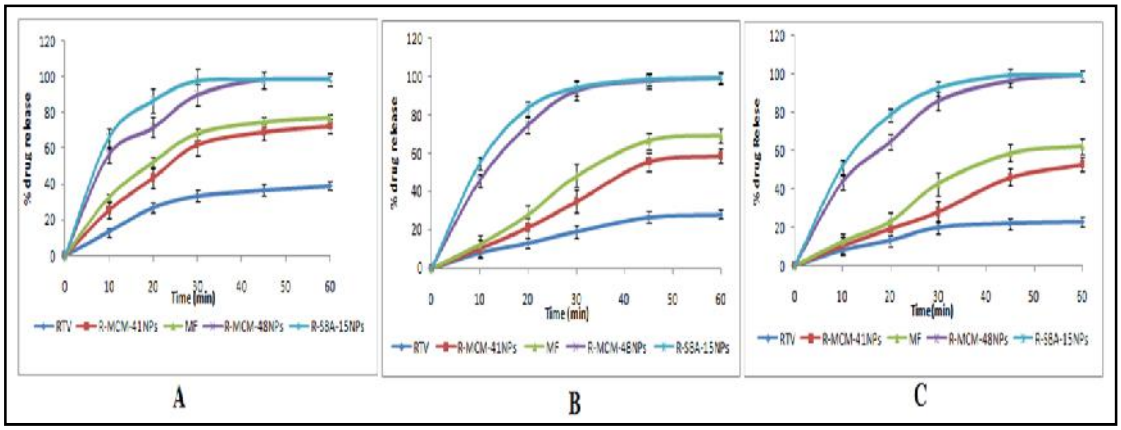

Figure 5.23 Release profile of RTV from pure RTV, R-MSNs and MF in (A) 0.1N HCl (B) pH 4.5 acetate buffer with 0.75 % PLE (C) pH 6.8 phosphate buffer with 0.75 % PLE

5.17 In-vivo study

RTV is a typical BCS II drug; whose absorption will be rate limited through the dissolution process. In the present study, the results of in-vitro dissolution studies were confirming the enhanced dissolution of RTV by R-MCM-48NPs, R-MCM-41NPs and R-SBA-15NPs (R-MSNs) compare to pure RTV. To study the silica nanoparticles effect, the in-vivo studies were performed in which the drug suspension was given orally to wistar rat. The results of plasma concentration-time profiles and the PK parameters of RTV are shown in Fig 5.24 and Table 5.7 respectively. In Fig.5.24 it is clearly shown that the absorption rate of R-MCM-48NPs and R-SBA-15NPs was higher than pure RTV, R-MCM-41NP and MF.

Drug plasma concentration profile of R-MCM-48Ps showed significant improvement in drug absorption compared to pure RTV and MF of RTV. Area under concentration-time curve (AUC_{0-t}) of RTV was found 26.55±1.84µg/mL*h for R-MCM-48NPs which was 1.94-fold and 1.38 fold higher with that of pure RTV (13.64±1.14 µg/mL*h) and MF of RTV (19.23±2.12 µg/mL*h) respectively. The maximum peak plasma concentration (Cmax) of RTV was found 9.62µg/ml for R-

MCM-48Ps which was about 2.48-fold and 1.54-fold greater than that of pure RTV (3.83±0.35 µg/ml/h) and MF of RTV (6.23±0.46 µg/ml/h), respectively.

Likely Drug plasma concentration profile of R-SBA-15NPs showed significant improvement in drug absorption compared to pure RTV and MF of RTV. Area under concentration-time curve (AUC_{0-t}) of RTV was found 23.96±1.04µg/mL*h for R-SBA-15NPs which was 1.75-fold and 1.24 fold higher with that of pure RTV (13.64±1.14 µg/mL*h) and MF of RTV (19.23±2.12 µg/mL*h) respectively. The maximum peak plasma concentration (Cmax) of RTV was found 8.94µg/ml for R-SBA15NPs which was about 2.33-fold and 1.43-fold greater than that of pure RTV (3.83±0.35 µg/ml/h) and MF of RTV (6.23±0.46 µg/ml/h), respectively. Time to reach maximum plasma concentration (T_{max}) for R-MCM-48NPs and R-SBA-15NPs was found to be 1 hour and for pure RTV and MF it was found 1.5 hrrespectively . Half life ($t_{1/2}$) of R-MCM-48NPs and R-SBA-15NPs was compared with pure RTV and marketed formulation of RTV, the $t_{1/2}$ for R-MCM-48NPs (1.80 ±0.12 h) and R-SBA-15NPs (1.84±0.17 h) was not found much dfferent than that of pure RTV (2.18±0.19 h) and MF of RTV (2.06±0.16 h).

The enhancement in AUC and C_{max} of R-MCM-48NPs and R-SBA-15NPs compared to pure RTV and MF of RTV could be due to the quick absorption of drug molecule by gastrointestinal wall due to the reduced particle size and incresed surface area followed by significantly improved dissolution rate, increased wettability and increase in adhesion surface area between nanoparticle and intestinal epithelium of villi which provides a direct contact with the absorbing membrane of the gut wall[56].

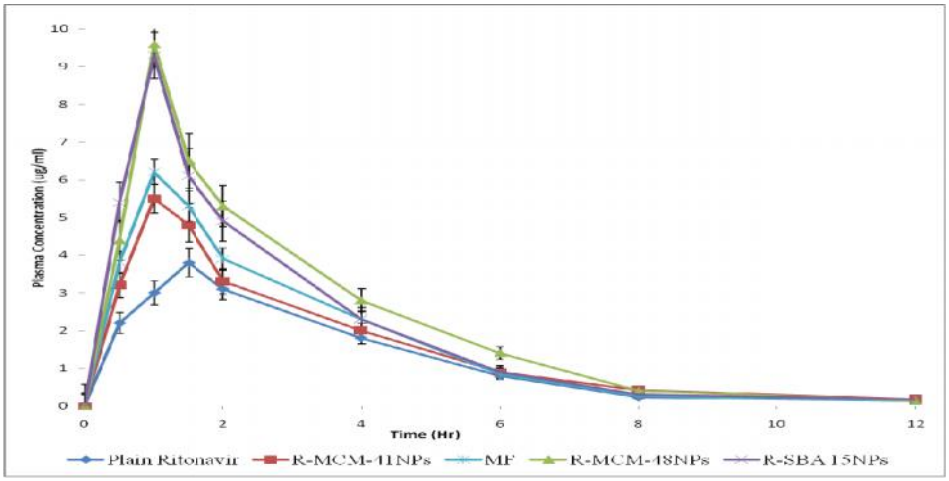

Figure 5.24 Graphical Representation of RTV plasma profile for pure RTV, R-MSNs and MF of RTV in Albino wistar rat following oral administration

Table 5.7 Pharmacokinetic parameter of RTV with different MSNs

Parameter	Pure RTV	R-MCM-41NPs	R-MCM-48NPs	R-SBA-15NPs	MF
C_{max}	3.83±0.35 µg/ml/h	5.54±0.72 µg/ml/h	9.62±0.77 µg/ml/h	8.943 ±0.62 ug/ml/h	6.23±0.46 µg/ml/h
T_{max}	1.5 h	1 h	1 h	1h	1h
AUC_{0-t}	13.64±1.14 µg/mL*h	18.29±1.77 µg/mL*h	26.55±1.84 µg/mL*h	23.965±1.64 µg/ml*h	19.23±2.12 µg/mL*h
$T_{1/2}$	2.18 h	2.16 h	1.80 h	1.84h	2.06±0.16 h

5.18 In vitro Cell Cytotoxicity Studies (MTT Assay)

Cytotoxicity study of RTV, RMCM-48NPs and R-SBA-15NPs was investigated in Caco2 cells by mitochondrial activity (MTT assay) to assess the safety/tolerability of prepared formulation on viability of cells. As Caco2 cells were used as absorption model, the biocompatibility and tolerability assessment of RTV and R-MCM-48NPs, R-SBA-15NPs on absorption barrier was necessary. After 48 h the % cell viability is more than 90 % at the concentration 500 µg/ml concentration of plain RTV and R-SBA 15 NPs, but slightly decrease the % cell viability in MCM-48NPs. (Fig.5.25) The surface area and particle size of mesoporous silica nanoparticles are important factors that affect the cell viability. The surface area of MCM-48NPs and SBA-15NPs was found to be 1220.29m2/g and 880.66 m2/g and pore size was 3.2nm and 5.9nm respectively. The avarage particle size of MCM-48NPs and SBA-15NPs was 100-200nm and 200-300nm respectively. It was found that small size and large surface area MCM-48NPs facilate more contact with cell than the large size and lower surface area[57,58] which may cause the slightly decrease the cell viability in MCM-48NPs. This confirms the biocompatibility of mesoporous silica nanoparticles and its composition did not contribute intoxicity of caco-2 cell.

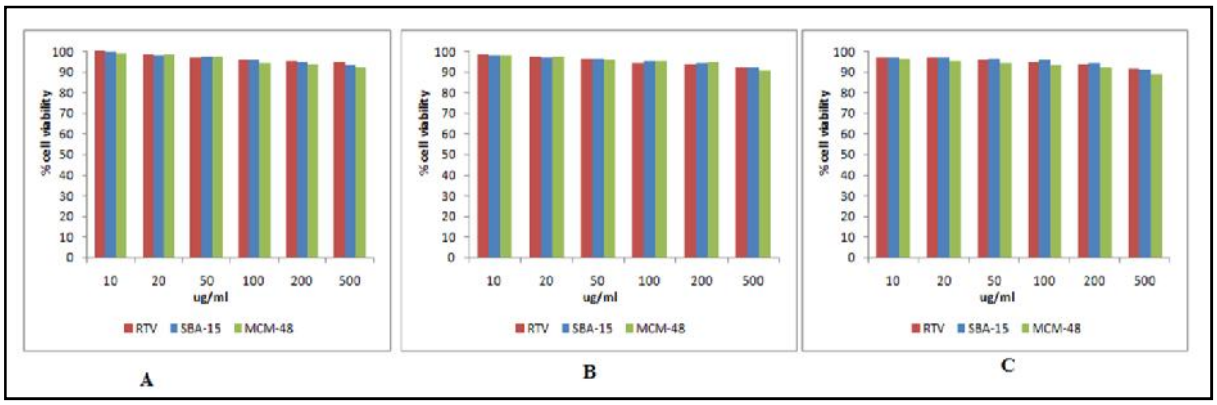

Figure 5.25 Cytotoxicity graphs for plain RTV and RTV loaded MCM-48NPs and SBA-15 NPs (A) 6h (B) 24h and (C) 48h

Conclusion

In vitro cytotoxicity study of drug loaded MCM-48 and SBA-15 MSNs on Caco-2 cell as a function of concentration and incubation time was demonstrated. The main difference between MCM-48 and SBA-15 MSNs was their surface morphology and chemistry. The results show that both the MSNs have different morphology and induced slight difference in in vitro cytotoxicity study. The slightly decrease in cell viability of caco-2 cell was more prominent when small size and larger surface area MCM-48 expose to higher concentration for longer duration of incubation. Under experimental condition it was found that both MSNs were biocompatible.

5.19 Stability Study

5.19.1 Physical Stability

The dissolution rate was significantly enhanced in drug loaded nanoparticles as compared to pure drugs. The argument for improvement in dissolution rate in silica nanoparticles was observed due to the conversion of drug into amorphous form after loading into mesoporous silica nanoparticles. So to verify the physical stability of R-MSNs at accelerated storage stability study was carried out.

With the increases in temperature, there is possibility that the bonding between drug molecules and carrier get broken because of increase in the molecular energy and motion within drug molecule. The changes in form of drugs after kept in accelerated storage condition for mentioned time were monitored by DSC and XRD analytical techniques, and structural physical stability of MSNs was monitored by TEM analysis.

5.19.1.1 P-XRD study of R-MSNs after accelerated storage condition

Powder XRD patterns of R-MCM-41NPs, R-MCM-48NPs and R-SBA-15NPs (R-MSNs) are shown in Fig. 5.26 A, B and C respectively. R-MSNs samples were stored at 40°C ± 2°C and 75% ± 5% relative humidity. The powder XRD patterns of all samples were recorded after 1, 3 and 6 months. The powder XRD of R-MSNs was taken at angle 2θ in the range of 5–50^{o} respectively and it did not shows any peaks relative to the crystalline RTV drug, that clearly indicated that RTV loaded in all MSNs are stable and not show any polymorphic change in drug

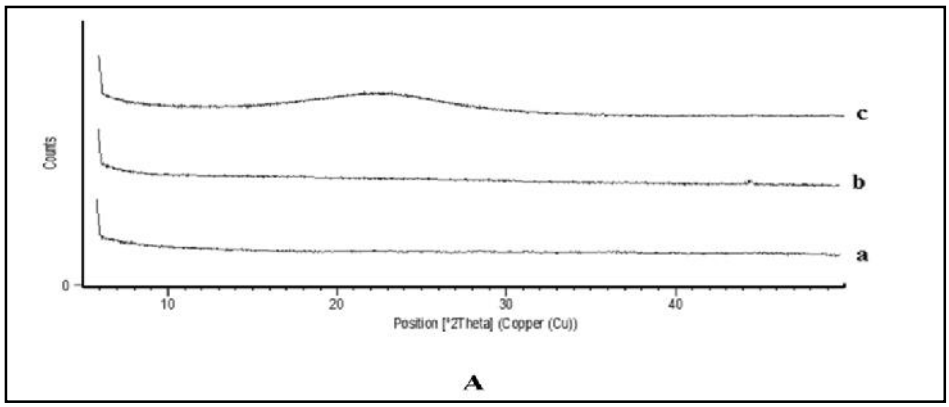

Figure 5.26 A: XRD pattern of R-MCM-41NPs in 40°C±2°C and 75%±5% relative humidity after A) 1 month, B) 3 month C) 6 month

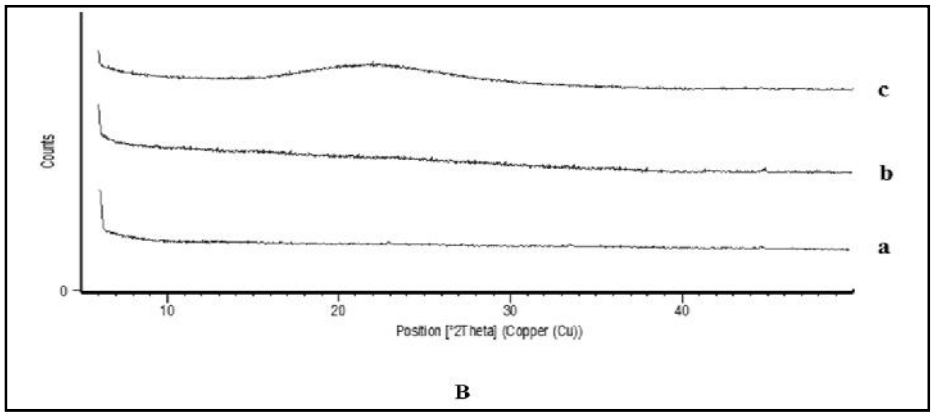

Figure 5.26 B: XRD pattern of R-MCM-48NPs in 40°C±2°C and 75%±5% relative humidity after A) 1 month B) 3 month C) 6 month

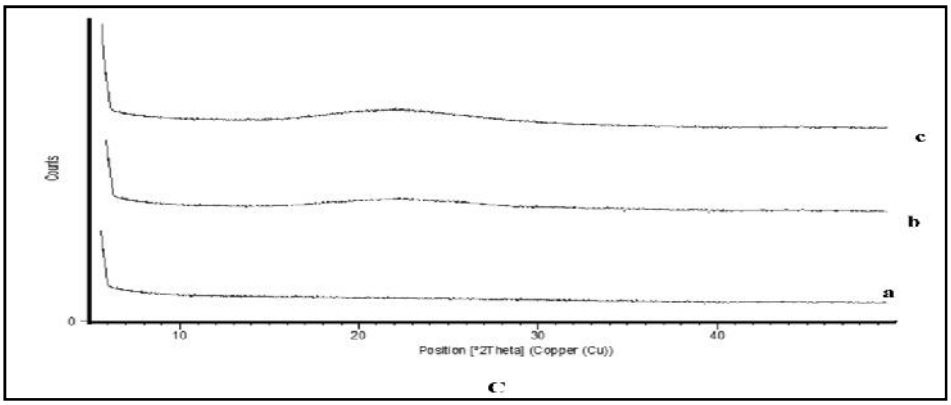

Figure 5.26 C: XRD pattern of R-SBA-15NPs in 40°C±2°C and 75%±5% relative humidity after A) 1 month B) 3 month C) 6 month

5.19.1.2 DSC study of R-MSNs after accelerated storage condition

DSC thermograms of R-MCM-41NPs, R-MCM-48NPs and R-SBA-15NPs (R-MSNs) are shown in Fig 5.27. R-MSNs samples were stored at 40 ◦C ± 2 ◦C and 75% ± 5% relative humidity. The DSC thermograms of all samples were recorded after storage of samples up to 1, 3 and 6 months. Fig 5.27 A, B and C shows DSC thermogram of R-MCM-41NPs, R-MCM-48NPs and R-SBA-15NPs at standard

DSC condition respectively. The stability of RTV within MSNs was proved as RTV fusion peak could not be detected at any thermogram of DSC. In DSC Thermograms broad peak around 70°C recorded due to loss of humidity and no fusion peak was observed at fusion point of RTV around 123ºC, The absences of fusion peak of RTV indicate that the RTV was completely loaded and physically stable within the pores of MSNs.

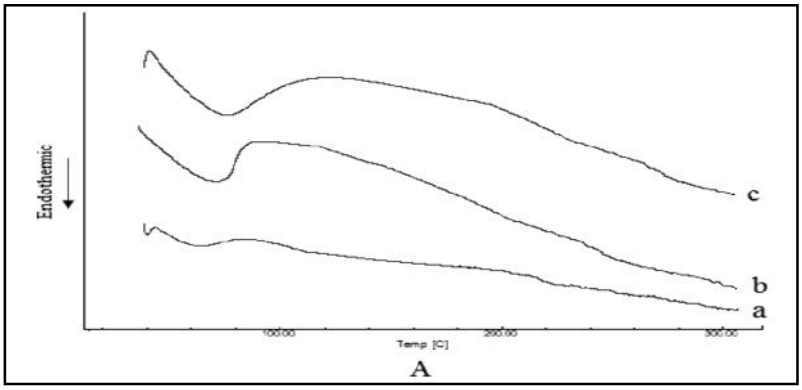

Figure 5.27A: DSC of R-MCM-41NPs (A) 40°C±2°C and 75%±5% relative humidity after a) 1 months b) 3 months c) 6 months

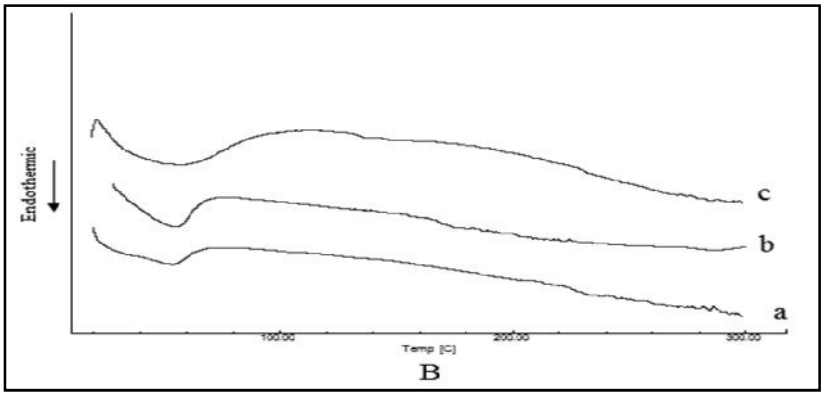

Figure 5.27 B: DSC of R-MCM-48NPs (A) 40°C±2°C and 75%±5% relative humidity after a) 1 months b) 3 months c) 6 months

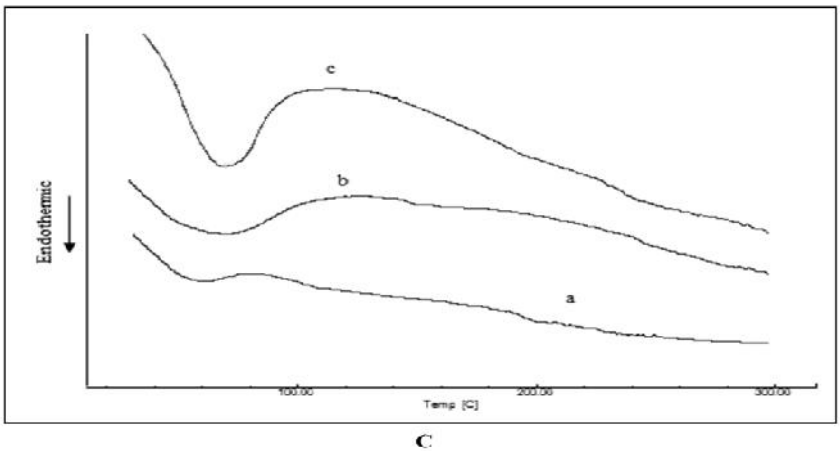

Figure 5.27 C: DSC of R-SBA-15NPs (A) 40°C±2°C and 75%±5% relative humidity after a) 1 months b) 3 months c) 6 months

5.19.1.3 TEM analysis

The physical storage stability of R-MCM-41NPs, R-MCM-48NPs and R-SBA-15NPs (R-MSNs) respectively were checked by TEM images. The mesoporosity of R-MSNs were observed and checked individually after kept in accelerated stability condition for 1, 3 and 6 months. In all tested conditions all the drug loaded MSNs show good physical stability and found no structural changes in all MSNs. Fig 5.28 A, B and C revealed the structural integrity of R-MSNs after 1, 3 and 6 months at 40ºC ± 2ºC and 75% ± 5% relative humidity respectively.

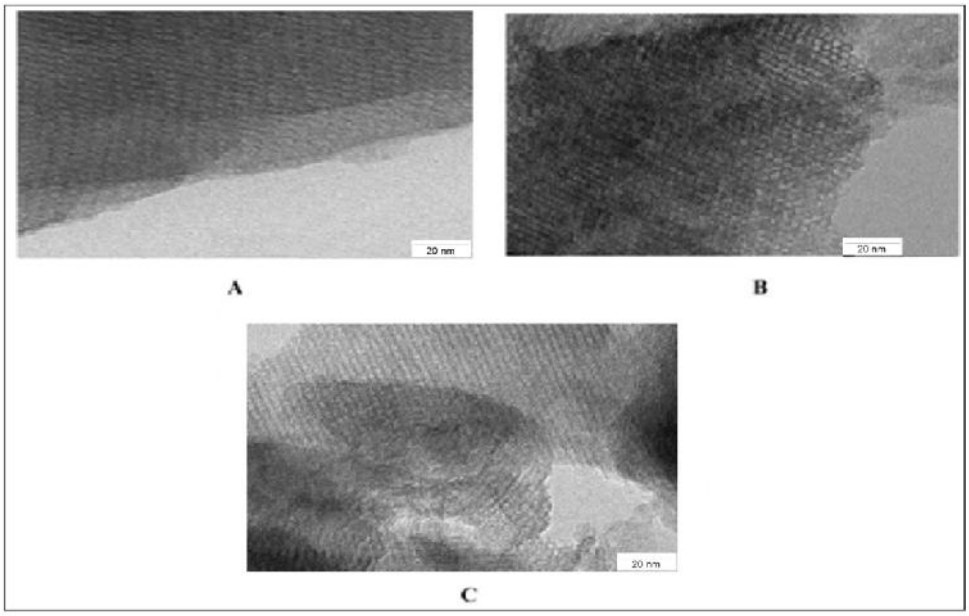

Figure 5.28 A: TEM images of R-MCM-41NPs in 40°C±2°C and 75%±5% relative humidity after A) 1 months B) 3 months C) 6 months

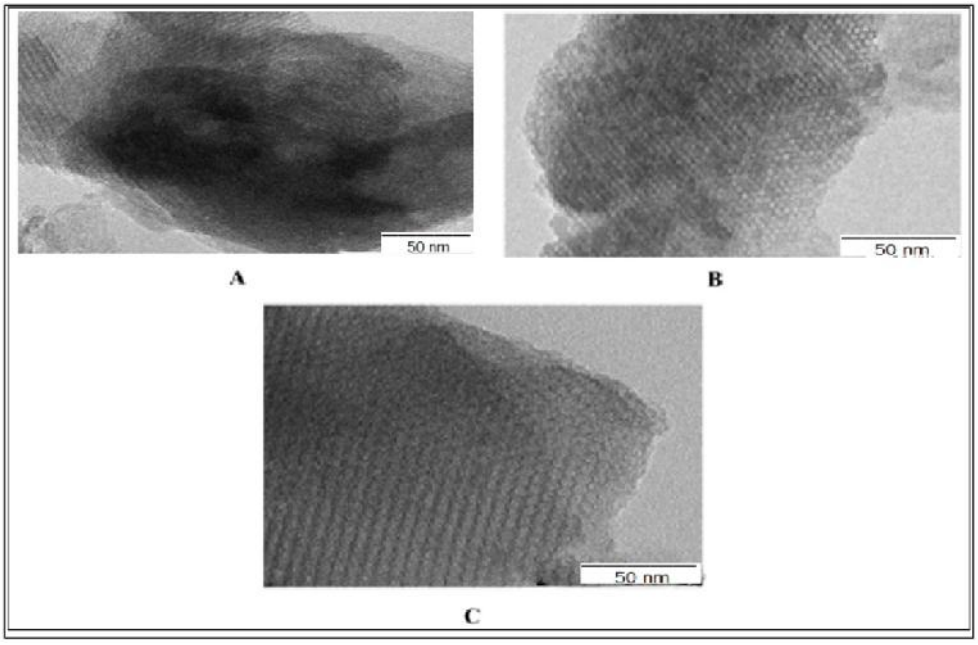

Figure 5.28 B:TEM images of R-MCM-48NPs in 40°C±2°C and 75%±5% relative humidity after A) 1 months B) 3 months C) 6 months

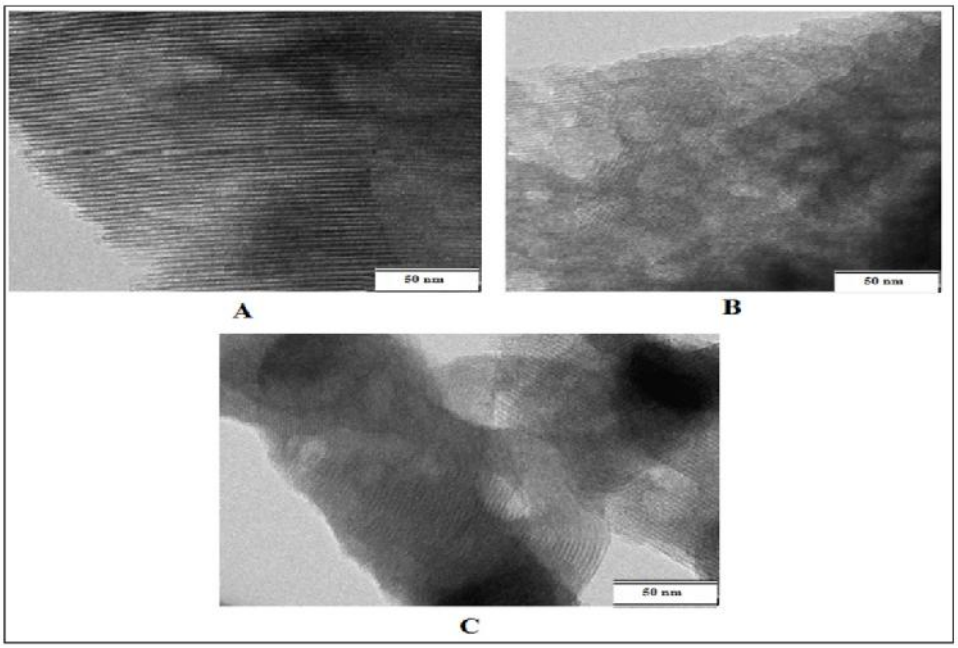

Figure 5.28 C: TEM images of R-SBA-15NPs in 40°C±2°C and 75%±5% relative humidity after A) 1 months B) 3 months C) 6 months

5.19.2 Chemical Stability

The Chemical stability of R-MCM-41NPs, R-MCM-48NPs and R-SBA-15NPs (R-MSNs) were checked by RP-HPLC. The chemical stability of drugs in MSNs was checked individually after kept in accelerated stability condition for 1, 3 and 6 the months samples. In all tested conditions all the drug loaded MSNs show good chemical stability and found no changes in content and concentration of drugs. The results are shown in table 5.8

Table 5.8 Chemical stability of R-MSNs (i.e. percentage drug content) at different time intervals, stored at 40°C ± 2°C and 75% ± 5% relative humidity

Sr. No.	Time	40°C±2°C and 75% ± 5% relative humidity	40°C±2°C and 75% ± 5% relative humidity	40°C±2°C and 75% ± 5% relative humidity
		% content of RTV in R-MCM-41NPs	% content of RTV in R-SBA-15NPs	% content of RTV in R-MCM-48NPS
1	Initial	99.58±0.79	99.90±0.35	99.58±0.79
2	1st Month	99.37±0.45	99.50±0.65	99.25±0.81
4	3rd Month	98.44±0.92	98.89±0.12	99.54±0.95
5	6th Month	98.35±0.88	98.49±0.78	99.08±0.59

* Data are shown as Mean±SD, n=3.

Conclusion

It was evident from DSC, XRD and TEM studies show that MCM-41NPs, MCM-48NPs and SBA-15NPs are stable carriers for RTV. Although humidity and water absorbed on the surface of MSNs have possibility to affect on the loaded drug in MSNs, but there were no crystallization changes and nucleation of drug occurred because of perfect match occurs between the drug molecule and MSNs pore diameter. Nucleation and crystallization of drug occur only when the diameter of carriers 20 times larger than the drug molecules. Therefore when drug molecule is perfectly enslaved in the pore of MSNs, its recrystaliization was prevented from both humidity and temperature.

Summery and Conclusion

In this study, the synthesized mesoporous silica nanoparticles MCM-41NPs, MCM-48NPs and SBA-15 were suitable carriers for poorly soluble RTV drug. RTV was loaded in all three silica nanoparticles to examine the effect of mesoporous size and geometry on solubility through the drug loading. To achieve maximum drug loading, solvent evaporation method was preferred with an appropriate ratio of RTV and carrier (1:1.5). (R-MCM-48NPs, R-MCM-41NPs and R-SBA-15NPs) In addition, characterization results like DSC, PXRD and N2 adsorption-desorption confirmed that the RTV was successfully loaded into the mesoporous silica nanoparticles. In in-vitro drug dissolution study, MCM-41NPs MCM-48NPs and SBA-15NPs showed several advantages as a carrier for drug delivery respectively. All silica carriers MCM-48NPs and SBA-15NPs could notably increase the dissolution rate of RTV as compared to the pure RTV, MCM-41NPs and MF but R-MCM-48NPs and SBA-15NPs showed better in the fast release.

In vivo assessment demonstrated that MCM-48NP and SBA-15NPs exhibited better pharmacokinetic properties compared to MCM-41NP, Pure RTV and RTV MF. The relative oral bioavailability of RTV in Albino wistar rat resulted from MCM-48NPs was found 2.48 and 1.54 fold greater than pure RTV and RTV MF, respectively. The reason behind the results is that MCM-48NPs having 3D cubic pores structure which offers easy drug diffusion from the interconnected pores into the dissolution media. From all the above facts revealed that MCM-48NPs contribute faster drug release as compared to MCM-41NPs with 2D hexagonal long channels. Thus, MCM-48NPs shows more propitious mesoporous carrier giving fast and maximum release compare with MCM-41NPs.

Likely from SBA-15NPs relative oral bioavailability of RTV was found 2.33-fold and 1.43-fold greater than pure RTV and RTV MF. Thus it can be concluded that that using mesoporous silica nanoparticles for RTV which leads to improved dissolution properties and excellent oral bioavailability of RTV.

SBA-15NPs also having 2D hexagonal long channels like MCM-41NPs but have high amount of silanol group present than MCM-41NPs, that adsorb more amount of RTV molecules and also SI-OH groups on SBA-15NPs form very weak bonding with RTV molecules as compared to MCM-41NPs, that can be easily and quickly broken down in dissolution media. Because of all these reasons SBA-15 NPs gave rapid dissolution as well as more diffusion in the dissolution medium.

In vitro Cell Cytotoxicity Studies (MTT Assay) confirmed the biocomatibility synthesised MSNs and explains that composition of MSNs did not contribute to toxicity of Caco2 cells.

Stability studiy results shows the RTV molecules showing good physical and chemical stability with in the mesopores and the mesopores carriers also shows good stability in accelarated conditions.

All these results shows mesoporous silica nanoparticles may give a new approach for the development of oral formulations for poorly water-soluble drugs like RTV.

References

1. Wouters BH, Chen T, Dewilde M and Grobet PJ: Reactivity of the surface hydroxyl groups of MCM-41 towards silylation with trimethylchlorosilane. Microporous Mesoporous Mater 2001; 44:453-457.
2. Schumacher K, Grun M and Unger K: Novel synthesis of spherical MCM-48. Micropor Mesopor Mater 1999; 27:201–206.
3. Zhao D, Feng J, Huo Q, Melosh N, Fredrickson GH, Chmelka BF, Stucky GD. Triblock copolymer syntheses of mesoporous silica with periodic 50 to 300 angstrom pores. Science 1998; 279:548-552.
4. Wei Y, Dattachowdhury B, Vangara KK, Patel N, Alexander K, Boddu SHS. Excipients That Facilitate Amorphous Drug Stabilization, Springer International Publishing Switzerland 2015; 463-495
5. https://aidsinfo.nih.gov/drugs/244/ritonavir/33/professional (access on dated 29/5/15)
6. Polli JE. In vitro studies are sometimes better than conventional human pharmacokinetic in vivo studies in assessing bioequivalence of immediate-release solid oral dosage forms. The AAPS journal 2008; 10: 289-299.
7. Tavelin S. et al. Prediction of the oral absorption of low-permeability drugs using small intestine-like 2/4/A1 cell monolayers. Pharm Res 2003; 20: 397-405.
8. Press B, Di Grandi D. Permeability for intestinal absorption: Caco-2 assay and related issues. Curr Drug Metab 2008; 9: 893-900.
9. Balimane PV, Han YH, Chong S. Current industrial practices of assessing permeability and P-glycoprotein interaction. AAPS J 2006; 8: E1-E13.
10. Rubas W. et al. Flux measurements across Caco-2 monolayers may predict transport in human large intestinal tissue. J Pharm Sci 1996; 85: 165-169.
11. Artursson P, Karlsson J. Correlation between oral drug absorption in humans and apparent drug permeability coefficients in human intestinal epithelial (Caco-2) cells. Biochem Biophys Res Commun 1991; 175: 880-885.
12. Artursson P. Cell cultures as models for drug absorption across the intestinal mucosa. Crit Rev Ther Drug Carrier Syst 1990; 8: 305-330.

13. Fogh J, Fogh JM, Orfeo T. One hundred and twenty seven cultured human tumor cell lines producing tumors in nude mice. J Natl Cancer Inst 1977; 59: 221-226.
14. Hidalgo IJ, Raub, TJ, Borchardt RT. Characterization of the human colon carcinoma cell line (Caco-2) as a model system for intestinal epithelial permeability. Gastroenterology 1989; 96: 736-749.
15. Pinto M et al. Enterocyte-like differentiation and polarization of the human colon carcinoma cell line Caco-2 in culture. Biol Cell 1983; 47:323-330.
16. Elsby R, Surry D, Smith V, Gray A. Validation and application of Caco-2 assays for the in vitro evaluation of development candidate drugs as substrates or inhibitors of P-glycoprotein to support regulatory submissions. Xenobiotica 2008; 38: 1140-1164.
17. Matsson P. et al. Exploring the role of different drug transport routes in permeability screening. J Med Chem 2005; 48: 604-613.
18. Alam MA, Mirza MA, Talegaonkar S, Panda AK, Iqbal Z. Development of Celecoxib Complexes: Characterization and Cytotoxicity Studies in MCF-7. Pharmaceut Anal Acta 2013: 4;1-8 .
19. American Type Culture Collection. in ATCC 30-1010K 1-6 (University Boulevard, Manassas, VA 20110 USA, 2011).
20. Spada G, Gavini E, Cossu M, Rassu G, Giunchedi P. Solid lipid nanoparticles with and without hydroxypropyl-β-cyclodextrin: a comparative study of nanoparticles designed for colonic drug delivery. Nanotechnology 2012; 23: 95-101.
21. Van Meerloo J, Kaspers GL, Cloos J. Cancer Cell Culture Vol. 731 Methods in Molecular Biology (ed Ian A. Cree) Ch. 20; Humana Press, 2011 237-245.
22. Khanavi M. et al. Cytotoxic activity of some marine brown algae against cancer cell lines. Biological research 2010; 43: 31-37.
23. Wang XD. et al. Permeation of astilbin and taxifolin in Caco-2 cell and their effects on the P-gp. Int J Pharm 2009; 378: 1-8.
24. Sieuwerts AM, Klijn JG, Peters HA, Foekens JA. The MTT Tetrazolium Salt Assay Scrutinized: How to Use this Assay Reliably to Measure Metabolie Activity of Cell Cultures in vitro for the Assessment of Growth Characteristics, IC50-Values and Cell Survival. Clin Chem Lab Med 1995; 33: 813-824.

25. Wallert and Provost Lab. 1-2 (Department of Chemistry and the Biochemistry and Biotechnology Program, University Moorhead, Minnesota 56563, Minnesota State, 2007).
26. Li AP. Screening for human ADME/Tox drug properties in drug discovery. Drug Discov Today 2001; 6: 357-366.
27. Zhou S, et al. Transport of the investigational anti-cancer drug 5, 6-dimethylxanthenone-4-acetic acid and its acyl glucuronide by human intestinal Caco-2 cells. Eur J Pharm Sci 2005; 24: 513-524.
28. Wang Z, Hop CE, Leung KH, Pang J. Determination of in vitro permeability of drug candidates through a Caco-2 cell monolayer by liquid chromatography/tandem mass spectrometry. J Mass Spectrom 2000; 35: 71-76.
29. Zheng J, Zhai S, Zhang Y, Wu D, Sun Y, Yang Y, Chen L, Deng F. Hydrothermally stable MCM-41 analogue with extensive embedded voids. Cat Today. 1998; 93-95, 529- 534.
30. Schulz-Ekloff G, Rathousky J, Zukal A. Controlling of morphology and characterization of pore structure of ordered mesoporous silica. Micropor Mesopor Mater. 1999; 27: 273–285.
31. Blin JL, Le´onard A, Su BL. Synthesis of large pore disordered msu-type mesoporous silicas through the assembly of surfactant and TMOS silica source: effect of the hydrothermal treatment and thermal stability of materials. J Phys Chem B 2001; 105: 6070-6079.
32. Bai N, Chi Y. Pang W. Influence of high pressure on structural property of mesoporous material MCM-41: study of mechanical stability. Materials Letters. 2002; 54: 37-42.
33. Trebosc J, Wiench JW, Huh S, Lin VSY, Pruski M. Solid-state NMR study of MCM- 41-type mesoporous silica nanoparticles. J Amr Chem Soc. 2005; 127: 3057-3068.
34. Nel A, Xia T, Madler L, Li N. Toxic potential of materials at the nano-level. Science 2006; 311: 622-627.
35. Miguel M, Marıa V. New developments in ordered mesoporous materials for drug delivery J Mater Chem. 2010; 20: 5593–5604.
36. Hamzah Z, Narawi N, MdRasid H, Md Yusoff AN. Synthesis and Characterization of Mesoporous Material Functionalized With Different

Silylating Agent and their Capability to Remove Cu2+. The Malaysian Journal of Analytical Sciences 2012; 16(3): 290 – 296

37. Zhang K, Yuan EH, Xu LL, Xue QS, Luo C, Albela B, Bonneviot L. Preparation of High-Quality MCM-48 Mesoporous Silica and the Mode of Action of the Template. European Journal of Inorganic Chemistry 2012;26:4183-4189.
38. Song SW, Hidajat K, Kawi S. Functionalized SBA-15 Materials as Carriers for Controlled Drug Delivery: Influence of Surface Properties on Matrix-Drug Interactions. Langmuir 2005; 21: 9568-9575.
39. QinY, Wang Y, Wang H, Gao H, Qu Z. Effect of morphology and pore structure of SBA-15 on toluene dynamic adsorption/desorption performance. Procedia Environmental Sciences 2013; 18 : 366 – 371
40. Taralkar US, Kasture MW, Joshi PN. Influence of synthesis conditions on structural properties of MCM-48. Journal of Physics and Chemistry of Solids 2008; 69:2075– 2081.
41. Ambrogi V, Perioli L, Pagano C, Latterini L, Marmottini F, Ricci M, Rossi C. MCM-41 for furosemide dissolution improvement. Microporous and Mesoporous Materials 2012: 147:343–349
42. Brunauer S, Emmet P, Teller E. Adsorption of gases in multi molecular layers. J Am Chem Soc 1938; 60: 309–319.
43. Wang Y, Sun L, Jiang T, Zhang J, Zhang C, Sun C, DengY, Sun J, Wang S. The investigation of MCM-48-type and MCM-41-type mesoporous silica as oral solid dispersion carriers for water insoluble cilostazol. Drug Dev Ind Pharm 2013: 1–10
44. Xu W, Riikonen J, Lehto V. Mesoporous systems for poorly soluble drugs. Int J Pharm 2013; 453: 181-197.
45. María V, Francisco B, Montserrat C, Miguel M. Drug confinement and delivery in ceramic implants. Drug Met Let. 2007; 1: 37-40.
46. Maria V, Francisco B, Daniel A. Mesoporous materials for drug delivery Angew Chem Int Ed. 2007; 46: 7548–7558.
47. Vallet-Regí M, Balas F. Silica Materials for Medical Applications. Biomedical Engineering Journal 2008; 2: 1-9

48. https://www.gograph.com/illustration/ritonavir-hiv-drug-protease-inhibitor-class-gg66342285.html

49. Salonen J, Laitinen L, Kaukonen AM, Tuura J, Björkqvist M, Heikkilä T, Vähä-Heikkilä K, Hirvonen J, Lehto V.P. Mesoporous silicon microparticles for oral drug delivery: loading and release of five model drugs. J Control Rel 2005; 108: 362–374.

50. Heikkilä T, Salonen J, Tuura J, Kumar N, Salmi T, Murzin D.Y, Hamdy M.S, Mul G, Laitinen L, Kaukonen A.M, Hirvonen J, LehtoV. Evaluation of mesoporous TCPSi, MCM-41, SBA-15, and TUD-1 materials as API carriers for oral drug delivery. Drug Deliv 2007; 14: 337–347.

51. Vasconcelos T, Sarmento B, Costa P. Solid dispersions as strategy to improve oral bioavailability of poor water soluble drugs. Drug Discov Today 2007; 12: 1068–1075.

52. Kesisoglou F, Panmai S, Wu Y. Nanosizing. Oral formulation development and biopharmaceutical evaluation. Adv Drug Deliv Rev 2007; 59: 631–644.

53. Jinno J, Kamada N, Miyake M, et al. Effect of particle size reduction on dissolution and oral absorption of a poorly water-soluble drug, cilostazol, in beagle dogs. J Control Release 2006; 111:56–64.

54. O'driscoll C, Griffin B. Biopharmaceutical challenges associated with drugs with low aqueous solubility – the potential impact of lipid-based formulations. Adv Drug Deliver Rev 2008; 60: 617–24.

55. Ambrogi V, Perioli L, Pagano C, Marmottini F, Ricci M, Sagnella A, Rossi C. Use of SBA-15 for furosemide oral delivery enhancement. Eur J Pharm Sci 2012; 46: 43–48

56. Ambrogi V, Perioli L, Pagano C, Marmottini F, Ricci M, Sagnella A, Rossi C. Use of SBA-15 for furosemide oral delivery enhancement. Eur J Pharm Sci 2012; 46: 43–48

57. Ma Y, Qi L, Ma J, Wu Y, Liu O, Cheng H. Large-pore mesoporous silica spheres: synthesis and application in HPLC. Colloids Surf. A 2003; 229: 1–8.

58. Xia D. et al. Preparation of stable nitrendipine nanosuspensions using the precipitation-ultrasonication method for enhancement of dissolution and oral bioavailability. Eur J Pharml Sci 2010: 40; 325-334.